U.S. DEPARTMENT OF COMMERCE
NATIONAL OCEANIC AND ATMOSPHERIC
ADMINISTRATION
NATIONAL WEATHER SERVICE

Environmental Modeling Center
Ocean Modeling Branch

TECHNICAL NOTE [1]

PARAMETERIZATION OF MIXING IN UPPER OCEAN

D. Chalikov, L. Breaker and L. Lobocki

December 9, 1996

[1]OMB contribution number No. 138

OPC CONTRIBUTIONS

No. 1. Burroughs, L. D., 1987: Development of Forecast Guidance for Santa Ana Conditions. National Weather Digest, Vol. 12 No. 1, 7pp.

No. 2. Richardson, W. S., D. J. Schwab, Y. Y. Chao, and D. M. Wright, 1986: Lake Erie Wave Height Forecasts Generated by Empirical and Dynamical Methods -- Comparison and Verification. Technical Note, 23pp.

No. 3. Auer, S. J., 1986: Determination of Errors in LFM Forecasts Surface Lows Over the Northwest Atlantic Ocean. Technical Note/NMC Office Note No. 313, 17pp.

No. 4. Rao, D. B., S. D. Steenrod, and B. V. Sanchez, 1987: A Method of Calculating the Total Flow from A Given Sea Surface Topography. NASA Technical Memorandum 87799., 19pp.

No. 5. Feit, D. M., 1986: Compendium of Marine Meteorological and Oceanographic Products of the Ocean Products Center. NOAA Technical Memorandum NWS NMC 68, 93pp.

No. 6. Auer, S. J., 1986: A Comparison of the LFM, Spectral, and ECMWF Numerical Model Forecasts of Deepening Oceanic Cyclones During One Cool Season. Technical Note/NMC Office Note No. 312, 20pp.

No. 7. Burroughs, L. D., 1987: Development of Open Fog Forecasting Regions. Technical Note/NMC Office Note. No. 323., 36pp.

No. 8. Yu, T. W., 1987: A Technique of Deducing Wind Direction from Satellite Measurements of Wind Speed. Monthly Weather Review, 115, 1929-1939.

No. 9. Auer, S. J., 1987: Five-Year Climatological Survey of the Gulf Stream System and Its Associated Rings. Journal of Geophysical Research, 92, 11,709-11,726.

No. 10. Chao, Y. Y., 1987: Forecasting Wave Conditions Affected by Currents and Bottom Topography. Technical Note, 11pp.

No. 11. Esteva, D. C., 1987: The Editing and Averaging of Altimeter Wave and Wind Data. Technical Note, 4pp.

No. 12. Feit, D. M., 1987: Forecasting Superstructure Icing for Alaskan Waters. National Weather Digest, 12, 5-10.

No. 13. Sanchez, B. V., D. B. Rao, and S. D. Steenrod, 1987: Tidal Estimation in the Atlantic and Indian Oceans. Marine Geodesy, 10, 309-350.

No. 14. Gemmill, W. H., T. W. Yu, and D. M. Feit 1988: Performance of Techniques Used to Derive Ocean Surface Winds. Technical Note/NMC Office Note No. 330, 34pp.

No. 15. Gemmill, W. H., T. W. Yu, and D. M. Feit 1987: Performance Statistics of Techniques Used to Determine Ocean Surface Winds. Conference Preprint, Workshop Proceedings AES/CMOS 2nd Workshop of Operational Meteorology. Halifax, Nova Scotia., 234-243.

No. 16. Yu, T. W., 1988: A Method for Determining Equivalent Depths of the Atmospheric Boundary Layer Over the Oceans. Journal of Geophysical Research. 93, 3655-3661.

No. 17. Yu, T. W., 1987: Analysis of the Atmospheric Mixed Layer Heights Over the Oceans. Conference Preprint, Workshop Proceedings AES/CMOS 2nd Workshop of Operational Meteorology, Halifax, Nova Scotia, 2, 425-432.

No. 18. Feit, D. M., 1987: An Operational Forecast System for Superstructure Icing. Proceedings Fourth Conference Meteorology and Oceanography of the Coastal Zone. 4pp.

No. 19. Esteva, D. C., 1988: Evaluation of Priliminary Experiments Assimilating Seasat Significant Wave Height into a Spectral Wave Model. Journal of Geophysical Research. 93, 14,099-14,105.

No. 20. Chao, Y. Y., 1988: Evaluation of Wave Forecast for the Gulf of Mexico. Proceedings Fourth Conference Meteorology and Oceanography of the Coastal Zone, 42-49.

Parameterization of mixing in upper ocean[2]

D. Chalikov[3]
University Corporation for Atmospheric Research, Boulder CO
L. Breaker
Environmental Modeling Center/NCEP/NWS/NOAA Washington DC
L. Lobocki [4]
General Sciences Corporation, Laurel, MD

Abstract

Because boundary layers with small thermal and mechanical inertias approximate steady-state conditions, the associated density and momentum fluxes tend to be constant with depth. As a result, these fluxes may be chosen as external parameters, and it then becomes possible to apply Monin-Obukhov similarity theory. For fluids with large thermal inertias such as the ocean, the density flux is a function of depth; thus, the external thermal forcing is no longer a governing parameter. In addition, if the mechanical inertia is also large, the structure of the boundary layer is not universal because it depends on the previous evolution of the thermal and mechanical forcing. However, if the mechanical inertia is small, the dynamical structure of the boundary layer adjusts almost instantaneously to the density structure and the mechanical forcing. This property allows us to generalize the Monin-Obukhov theory for stratifiedboundary layers through specification of a stratification parameter which characterizes the internal density structure instead of the external density flux. The thermal time scale for the upper ocean is relatively large whereas the dynamical time scale is 1-2 orders of magnitude shorter. Consequently, the upper ocean may be considered steady-state in a dynamical sense and any dynamical property depends primarily on the depth, surface momentum flux, and the vertical density structure. Based on this assumption, we can choose the appropriate scaling for the turbulent mixing coefficient. A nondimensional turbulent mixing coefficient is derived which depends on the stratification parameter which, in turn, includes the surface stress and the integral density deficit for the entire layer above. The

[2] Ocean Modeling Branch contribution No. 112.

[3] *Corresponding authors address:* National Environmental modeling, 5200 Auth Road, Washington DC 20233

[4] Warsaw University of Technology, Poland

general form and asymptotic behavior of the nondimensional turbulent mixing coefficient as a function of the stratification parameter is formally obtained using dimensional considerations. Its structure is determined using empirical data obtained in the atmospheric boundary layer. The final formulation is based on 8 years of temperature profiles acquired at Ocean Weather Ship (OWS) PAPA. This approach reproduces the 8-year evolution of the upper ocean with a maximum rms difference of approximately $1\ K$ and a bias of $1\ K$ over the depth range of 0-150m. An additional 1-year simulation of the upper ocean at OWS CHARLEY and a 9-year simulation at OWS NOVEMBER suggest the universal nature of t is approach. Overall, the simple turbulent mixing scheme which is derived reproduces the evolution of the upper ocean with accuracies similar to those obtained using more complicated models. Related problems of sea surface temperature data assimilation and its predictability are also considered. In addition, an investigation of mixed layer deepening forced by constant wind and mass exchange is performed. Finally, estimates of the influence of vertical resolution on the accuracy of model simulations are obtained.

1. Introduction

The most important ocean characteristics which is responsible for ocean-atmosphere thermodynamic interaction is sea surface temperature (SST). The primary spatial and temporal variations in temperature are concentrated in a seasonally-active upper layer, whose depth is mainly determined by the amplitude of the seasonal variations in mass exchange, intensity of wind mixing, and vertical motion. This active layer is usually topped by a so-called mixed layer (ML), where vertical gradients of temperature are very small. The physics of ML are similar to that of atmospheric surface layer but with specific features which are different due to high thermal inertia of water (see discussion in section 2). Assuming that vertical fluxes of heat and momentum in the atmospheric surface layer are of the same order, we can estimate that ratio r of vertical temperature differences in water ΔT_w and in air ΔT_a

$$r = \frac{\Delta T_w}{\Delta T_a} = \frac{c_a}{c_w}\sqrt{\frac{\rho_a}{\rho_w}} \tag{1}$$

(c_w, ρ_w and c_a, ρ_a are specific heat capacity and density of water and air correspondingly) is of order 0.01. This does not mean, however, that stratification the ML is neutral, because the ratio of Monin-Obukhov scales for water L_w and for air L_a are

$$\frac{L_w}{L_a} = (\alpha T)^{-1}\frac{c_w}{c_a}\sqrt{\frac{\rho_a}{\rho_w}} \tag{2}$$

($\alpha \simeq 2 \cdot 10^{-4} C^{-1}$ is a coefficient of thermal expansion of water) and turns out to be of order 1, and thus the role of stratification in the ML is comparable to that in the atmospheric surface layer. Consequently, the ML may be considered homogeneous only in a sense that the gradients of temperature here are much less than it is below the ML in the upper thermocline, where the temperature gradient is large (approaching values of 1 Km^{-1}) and the Richardson number (Ri) is usually high. Nevertheless, even under very stable conditions, the heat and mass fluxes still greatly exceed those which result from molecular diffusion, and significant variations in temperature in upper thermocline are usually observed. Therefore, without considering heat transfer in upper themocline, it is not possible to reproduce the variations

of SST. Although the mechanism of heat exchange between ML and upper thermocline is understood poorly, several processes are most likely responsible for producing vertical heat exchange between ML and upper thermocline (Large et al, 1994, Garret, 1995):

1. After the decrease in dynamical forcing or an increase in heating, new discontinuities in density form which result in the trapping of lower part of ML and its assimilation into upper thermocline.

2. Pure turbulent entrainment is produced by intense mechanically-generated or convective turbulent eddies due to strong winds and/or surface cooling.

3. Mixing is produced by breaking of internal waves. Measurements show that this type of mixing is always present in ocean interior (Gregg, 1987). The ensemble effect of this intermittent turbulence produces a momentum and heat exchange between ML and upper thermocline and vertical fluxes in ocean interior.

4. Mixing is produced by surface waves. Nonlinear surface waves can produce mixing and also internal waves which finally break, creating turbulence.

5. Mixing is produced by irreversible components of secondary motions such as Langmuir circulation, resuling from dynamic instability of ML which may be coupled to the surface waves.

Because SST is very sensitive to vertical mixing in upper layer, ocean models should clearly be able to parametrize this process. Generally, the term *'parameterization'* may be defined as a formulation of rules for modeling the subgrid processes responsible for energy transformations in terms of the large-scale variables. For ocean models, 'large-scale' corresponds to variables which are averaged over 4-D space-time boxes with horizontal size of order of 1-100 km, vertical size of order of 1-10 m and time intervals of order 1 min-1 hour. The specific feature of upper ocean is its well pronounced fine structure and multiscale space and temporal variability (Monin et al. 1977, Fedorov XXX),. Horizontally averaged fields loose this structure and thus oversimplify the real processes. This dramatic gap between ocean model scales and the actual scales observed 'in situ' reduces the parameterization

problem to purely phenomenological, consisting of the construction the empirical relationships between averaged external forcing and related large-scale variations of the upper ocean. Thus, observational data which are needed to formulate and validate various parameterizations should encompass large time and space scales. Space-averaged data (except for remotely sensed SSTs) are usually unavailable, and so, long series of temperature, salinity (and current) profiles should be used. Such data have only been obtained at Ocean Weather Stations (OWS), where where long-time series of temperature profiles were obtained. Most models of of the ML have been developed using these data in spite of their relatively low accuracy.

A simulation of upper ocean is based on heat conductivity equation. [5]

$$\frac{\partial T}{\partial t} = -\frac{\partial \overline{w'T'}}{\partial z}, \tag{3}$$

where u, u', w', T' have standard definitions, and the axis z points up.

Eq. (3) assumes horizontal homogeneity. In general case, this equation should incorporate the effects of 3-D advection and horizontal mixing, thus, Eq. (3) may be also treated as a 'submodel' of a general circulation ocean model which uses numerical splitting method.

Models of upper ocean may be divided into two groups: (1) *parametric* and (2) *differential.* In *parametric* (or so-called 'bulk') models, the general structure of upper ocean is assumed to be known, and as a result equations can be derived for the parameters describing this structure. The *parametric* models take their origin from Kraus and Turner (1967) which first introduced the concept of a mixed layer characterized by temperature and depth, and then derived the equations for describing its evolution.Most parametric models contain only the following parameters: depth of mixed layer h, its temperature T_s, and certain characteristics of upper thermocline which are assumed to be known: temperature difference at the bottom of mixed layer $T_s - T_h$, or vertical temperature gradient in upper thermocline $\left(\frac{dT}{dz}\right)_{h+0}$, or

[5] For simplicity, we consider in this introduction only thermal processes but generally upper ocean models should take into account salinity as well. Volume heating by shortwave radiation is also neglected

both these parameters. One evolutionary equation may be obtained by integrating (3) over depth up to $z = h$ taking into account the variability of h.

$$h\frac{\partial T_s}{\partial t} = -(T_s - T_h)\frac{dh}{dt} - \overline{w'T'} \mid_{z=0} + \overline{w'T'} \mid_{z=h} \tag{4}$$

Here T_h is the temperature at the botom of ML. First term in (4) describes the heat exchange between ML and underlying thermocline produced by displacement of lower boundary of ML. This term can be interpreted only when $\partial h/\partial t > 0$. In the opposite situation when $\partial h/\partial t < 0$, a formal use the (4) would assume that process inverse to mixing occurs, when cooled by $T_s - T_h$ water is transfered to the underlying region. Instead, Kraus and Terrner (1967) suggested that entrainment in this case is absent. In reality, the depth of ML may decrease through the formation of a new temperature discontinuity in the ML arising when the wind weakens or heating increases. Often, a new temperature discontinuity moves down and reaches a base of the ML. The term $-\overline{w'T'} \mid_{z=0}$ represents the kinematic heat exchange through the surface [6], and $-\overline{w'T'} \mid_{z=h}$ describes heat diffusion through the bottom of ML at $z = -h$. Since this term is unknown, further assumptions are related to its parameterization.

A simple way to derive an additional equation consists of multiplying equation(3) by z and again integrating over depth. As a result, we obtain an equation for a quantity which is proportional to potential energy for a unit column of depth h:

$$\frac{h}{2}\frac{\partial T_s}{\partial t} + (T_s - T_h)\frac{\partial h}{\partial t} = \overline{w'T'} \mid_{z=h} - \int_{-h}^{0} \overline{w'T'}dz \tag{5}$$

This equation again contains unknown variables $T_s - T_h$, $\overline{w'T'} \mid_{z=h}$ and the term $\int_{-h}^{0} \overline{w'T'}dz$ which is proportional to a mutual transformation of potential energy and kinetic energy of tutbulence. This term may be obtained from integrating the equation of kinetic energy of turbulence over the depth of ML. This equation introduces dynamic forcing through the action of wind sress and turbulent energy flux from dissipating waves. Unfortunately, the

[6] Strickly speaking, due to surface kinematic boundary condition, this term becomes zero at interface. Thus, heat exchange through the surface may occur by molecular conductivity (and also from incoming solar radiation and by sprays)

final equations cannot be derived formally because equation for turbulent energy contains nonlinear production and dissipation terms and last of them has singularity near the surface. Thus, the relations so obtained are qualitative, leaving ample room for different 'ad hoc' constructions. As a result, a large number of schemes for parameterizing the oceanic and atmosheric mixed layers have appeared.

Kitaigorodskii and Miropolskii (1970) used a different approach for parametrizing the strucrure of seasonally active layer based on similarity considerations. They assumed that continuous temperature profiles in seasonal active layer may be described as

$$T = \begin{cases} T_s, & z \le h_m \\ T_s - (T_s - T_a)M(\zeta), & h_m < h < h_a \end{cases} \tag{6}$$

where unknown variables are still ML depth, h_m, and the ML temperature, T_s. The external parameters are depth of the seasonally active layer h_a and the temperature at the bottom T_a of this layer, which are assumed to be known or can be derived from a large-scale ocean model. $M(\zeta)$ in (6) is an empirical nondimensional function of nondimesional depth $\zeta = (z-h)/(h_a - h_m)$, approximated as

$$M(\zeta) = \frac{8}{3}\zeta - 2\zeta^2 + \frac{1}{3}\zeta^4 \tag{7}$$

Relations (6), (7) embrace a large variety of temperature profiles in upper ocean. Advantage of this approach is that: (1) due to discontinuity of temperature profile (6) within the active layer, no hypothesis for turbulent entrainment is required, and (2) variability of T_a is much less than that of T_h in previous scheme. Of course, uncertanties arising from the integration of the turbulent energy equation over depth arise here also.

Because all parametric schemes use many arbitrary assumptions, this approach may be considered as a pure heuristic, based mostly on empirical data. Numerous calculations (see review by Large et al. 1994) showed that after appropriate tuning [7] bulk models (based sometimes on different assumptions)

[7] A delicate process consisting of modifying the formulation of a model to obtain better results and also indirectly to take into account effects which were not included. Models which need tuning for simulating different data sets cannot be used for parameterizing.

are able to reproduce the evolution of temperature and depth of mixed layer satisfactorily. An advantage of this approach is its computational efficiency. The mathematical formulation of these models is simple, and it may be fully analysed for obtaining fast computing and robust numerical scheme. Nevertheless, there are disadvantages of this approach also:

1. Oversimplification of the structure of upper ocean. In reality, temperature profiles are continuous, so, the definition of h_m and $T_s - T_h$ (or T_a and h_a) cannot be made objectively.

2. Oversimplifying the heat exchange mechanisms between ML and upper thermocline, and neglecting thermal conductivity in the upper thermocline.

3. Inconsistencies arise with differential formulations of ocean models. If gridded vertical temperature profiles are treated as step functions, it is unclear which temperature discontinuity corresponds to the lower boundary of ML. Truncated temperature profiles with the same accuracy may be treated also as continuous functions, thus, the ML depth cannot also be derived objectively again. As a result, the uncertainties arise in combining differential ocean models with bulk model of upper ocean.

In fact, the bulk models are well suited for describing the evolution of ML per se but they do not fully describe the evolution of upper ocean which results from turbulent exchange between ML and upper thermocline.

The altenative approach, based on differential equations and closure hypotheses, may be applied formally for the evolution of the entire upper ocean. Nevertheless, the applicability of this approach to modeling turbulent entrainment and vertical diffusivity in upper thermocline is very questionable.

It is well known that all models of turbulent flow which are based on the Friedman-Keller equations (Monin and Yaglom, 1971) assume the existence of fully-developed turbulence which produces a cascade of energy from the mean flow to large and small eddies. The presence of fine structure and the almost complete absence of turbulence below ML shows that these fundamental assumptions are violated. Thus, models which are based on closure schemes are realistic only within ML and within turbulent patches

which arise, for example, from breaking the internal waves. It should not be assumed that the equations for diffusion of temperature and momentum together with the equation for turbulent energy, rate of dissipation, lenght scales relationships, etc, can adequately describe the processes of entrainment and mixing under stable stratification. First, the effects of intermittency of mixing, statistical dynamics of internal waves and coherent structures are completely not represented in any turbulent closure model. Second, all of these systems of equations predescribe the dissapearance of turbulence when the rate of the transformation of turbulent kinetic energy to potential energy approaches to the rate of generation. This is true from the point of view of conventional theory of turbulence, but it is not correct physically, because turbulence in this case continues to act, but in a transformed and poorly understood manner (e.g. Gregg, 1987, Muller, 1993). Also, it is unlikely that by adding more complexity to existing closure schemes is possible to reach better results.[8] If these models are applied to entire upper ocean, they are likely to fail, because they ignore the specific physics of mixing under stable stratification, which, however, is taken into account in the bulk models.

It may be shown that numerical models of ML based on differential approach in some cases do not approximate an initial differential equations. Here we consider only one aspect of the problem - turbulent entrainment at the base of ML. Assume that a mixing model, based on an appropriate closure scheme, is able to describe the general features of turbulence for small positive Ri numbers. As we approach to to the upper thermocline, Ri continues to increase, and eventally reaches the critical value Ri_{cr} where the turbulent coefficient approaches zero or is replaced by some small 'residual' value, which is essentially a tuning parameter. During periods of heating when the ML is well pronounced and upper thermocline has a sharp gradient, this transition occurs very quickly, sometimes within a single vertical step in a numerical model. In this case, the evolution of the depth of ML depends completely on the details of the numerical scheme. In schemes where the gradient of temperature and the turbulent coefficient are calculated at

[8]For example, Kantha and Clayson (1995) recently suggested a scheme consisting of 6 highly complicated equations supplemented by about 20 additional differential expessions. The equations contain 10 so-called 'constants'. This 'submodel' is more complicated than complete ocean model, and, due to its high order, requires hundreds of gridpoints. This model cannot be fully investigated and its solution may fall into unwanted regimes.

the same point, the rate of displacement for discontinuties depends only on a residual value for turbulent coefficient, thus, it has been introduced manually. In most models, this effect is hidden because staggered grids are used. For such scheme temperature diffusion near density discontinuities is produced not by the limiting value for K but by half of the sum of this value and the adjacent value, which may be not small. Heat transfer is thus enhanced in the upper thermocline, and its value becomes crucially dependent on vertical resolution. Thus, under the same forcing, the depth of ML can grow quickly for coarse resolutions and does not change for fine resolutions (when residual value of K is equal to zero). Thus, the key mechanism for ML evolution is not adequately reproduced in turbulent closure models. Of course, some artificial modifications may be taken to reduce this effect, but in this case precisely these modifications obtain the main importance, and turbulence model itself works only above the entrainment level in ML where mixing is relatively simple. Of course, differential models also may be tuned, but comparison of such models with bulk ML models does not show that either type has obvious advantages. (Martin, 1985).

Thus, we conclude that in both approaches the exchange of heat and mass between the ML and the seasonal thermocline remains an obscure issue. Obviously, it is impossible at present to derive a physical model which describes from first principles the ensemble effect of all processes which may be responsible for vertical mixing in the upper layer. This is why we propose a simple phenomenological approach consisting of the analysis of resulting effects of different and poorly understood processes, in terms of an effective heat conductivity coeffficient. Our approach to quantify mixing in the upper ocean is based on a modification to the similarity theory of Monin and Obukhov. This approach is also somewhat analogous to a nonlocal parameterization of turbulent mixing applied to the atmospheric surface layer by Troen and Mahrt, (1986) and recently applied to the oceanic ML by Large et al. (1994). Taking into account the large thermal inertia of the ocean, we have introduced a new nonlocal stratification parameter which makes possible a realistic and very simple description of mixing in the ML and the upper thermocline.

2. Similarity considerations

Similarity theory (Obukhov, 1946; Monin and Obukhov, 1954) has been used extensively to describe the atmospheric surface layer (ASL). However, the general basis for similarity theory must be revised for application to the ocean. Consider the ASL with height $h \simeq 10\ m$ whose structure is governed by the wind stress τ and the surface heat flux H multiplied by a buoyancy parameter $\frac{g}{T}$ (g is the acceleration of gravity and T is the absolute temperature in K). The averaged equations for temperature and momentum evolution are

$$\frac{\partial T}{\partial t} = \frac{\partial \overline{w'T'}}{\partial z}, \tag{8}$$

and

$$\frac{\partial u}{\partial t} = \frac{\partial \overline{w'u'}}{\partial z}. \tag{9}$$

where u, u', w', T' have standard definitions. These equations allow us to estimate the dynamical (T_{da}) and thermal (T_{ta}) time scales as

$$T_{da} = \frac{\rho_a U_a h}{\tau}, \quad T_{ta} = \frac{c_a \rho_a \Delta T h}{H}, \tag{10}$$

where U_a is the wind velocity, τ and H are the surface stress and heat flux, respectively, ΔT is the vertical temperature difference across the surface layer ($\simeq 1 - 2\ K$), ρ_a and c_a are the density and specific heat capacity of air, respectively, and h is a height scale for the ASL. With appropriate values of $\tau \simeq 0.3\ Nm^{-2}$, $H \simeq 10 - 100\ Wm^{-2}$ and $h \simeq 10\ m$, (10) gives values for $T_{da} \simeq T_{ta} = 10^2 - 10^3$ s. These time scales indicate that for periods $\geq T_{da}$ and T_{ta}, the thermal and the dynamical structure of the surface layer may be considered to be steady-state. The relatively small thermal and mechanical inertias of the surface layer produce a rapid response to external forcing which explains why Monin-Obukhov similarity theory was generally successful when applied to the lower atmosphere.

Next, we estimate similar time scales for the upper oceanic boundary layer. If we assume that τ and H are the same for both media, then

$$T_{dw} = \frac{\rho_w U_w h}{\tau}, \quad T_{tw} = \frac{c_w \rho_w \Delta T h}{H}. \tag{11}$$

For a vertical temperature difference $\Delta T \simeq 1\ K$ and a surface current velocity $U_w \simeq .03U_a$ and a layer depth $h \simeq\ 10\ m$, the corresponding time scales for T_{dw} are $\sim 10^4$ s and $\sim 10^5 - 10^6$ s for T_{tw}.

As expected, the time scales for the ocean greatly exceed those for the atmosphere. This difference is due to the greater density and heat capacity of water which acts to decrease the rates of momentum and heat evolution. Thus, the steady-state assumption for thermal structure is formally valid only for layer depths of the order of 1-10cm. However, this scale is meaningless in the presence of waves; thus, Monin-Obukhov similarity theory cannot be applied directly to the upper ocean.

A second property of the oceanic boundary layer, which distinguishes it from the ASL, is the large difference between the dynamical and thermal time scales (1-2 orders). This difference arises because the ratio of heat capacity to density is larger for water than it is for air, and because oceanic motions are smaller than atmospheric motions by almost two orders of magnitude.

These scale differences imply that dynamical adjustment of the upper ocean occurs 1-2 orders of magnitude faster than it does for thermal adjustment. A representative value for the dynamical time scale is of the order of several hours. A typical period for significant changes to occur in the atmosphere varies from one to several days; thus, in a dynamical sense, the upper ocean is approximately steady-state. However, the thermal state of the upper ocean is essentially unsteady. As a result, the heat flux is a function of depth and its surface value is not a governing parameter as was assumed when similarity theory was applied to the atmosphere. On the other hand, the surface stress is an important external parameter due to the relatively short dynamical time scale in the oceanic case.

Consider the evolution of the upper oceanic layer with a characteristic depth $h << L$ where L is a horizontal length scale $\cong 10^4 - 10^5\ m$ with a time scale $> T_{dw}$. We assume that kinetic energy is acquired at these scales only from the surface above. The stratification of the upper layer is described by its vertical density distribution $\rho(z,t)$. We now formulate the similarity hypothesis: for steady-state flow, any dynamical property $D(z,t)$ (e.g., turbulent energy, its rate of dissipation, or the turbulent mixing coefficient) may

be represented in the following form

$$D(z,t) = D_*(t) F_D \left(\frac{g}{\rho_0} \rho(z,t), v_*, z \right) \tag{12}$$

where ρ_0 is the mean density of sea water, D_* is an appropriate scale (having the same dimension as D), $v_* = \sqrt{(\tau/\rho_w)}$ is the water friction velocity, and F_D is a function describing the joint influence of dynamical forcing and stratification. The density profile $\rho(z)$ may be represented by a sufficient number of moments of the form $\int_0^z (\rho(y) - \rho(0)) y^n dy$ $(n = 1, 2, 3...)$. As a first approximation we assume that the stratification can be represented with reasonable accuracy by a moment of low order. A suitable nondimensional stratification parameter, S_p, may be expressed, for example with $n = 1$, as

$$S_p = \frac{\frac{g}{\rho_0} \int_0^z (\rho(z') - \rho(0)) z' dz'}{z v_*^2}. \tag{13}$$

This parameter represents (to within an arbitrary numerical factor) the ratio of the potential energy of the layer to its kinetic energy. It is positive for stable stratification and vice versa. Monin-Obukhov similarity theory may now be applied in terms of this integral parameter. We can replace the instantaneous values of heat flux by a single parameter which characterizes the entire layer above. This approach represents a reformulation of Monin-Obukhov theory since any result based on this theory can also be expressed in terms of the integral parameter, S_p. For example, the turbulent mixing coefficient, K_T, may be expressed as

$$\tilde{K_T} = \frac{K_T}{\kappa v_* (z + z_0)} = \left(\zeta \frac{\partial F_T}{\partial \zeta} \right)^{-1} \tag{14}$$

where F_T is a function which approximates a nondimensional temperature profile, $\zeta = \frac{z}{L}$ is a nondimensional height, and L is the Monin-Obukhov length scale given by

$$L = \frac{v_*^3}{\kappa \frac{g}{\rho_0} \overline{w' \rho'}} \tag{15}$$

(See Monin and Yaglom (1971) for details). When $z = 0$, the turbulent mixing coefficient equals $\kappa v_* z_0$. This formal result is useful for approximating temperature profiles for depths where $z >> z_0$. For wind profiles above the

sea surface, z_0 is of the order of $10^{-4}m$.

The dynamical and thermal structure of the ML depends primarily on the conditions which exist at the ocean surface. For winds $< 5ms^{-1}$, the ocean surface is relatively smooth and no wave breaking occurs. In this case, the surface kinematic boundary condition is valid for all scales and heat transfer is maintained by molecular processes. When winds exceed $5 - 8ms^{-1}$, the ocean surface becomes unstable and wave breaking occurs. In this case, heat (and momentum) exchange across the ocean surface is far more intense than it would be for a smooth surface. [9] We assume that a well-mixed subsurface layer is formed over the depth h_s which is $\sim 1\ m$. For steady-state wave fields, a unique length scale $\Upsilon = v_*^2/g$ can be obtained from the Charnock (1955) relation where we assume that the penetration depth h_s is proportional to Υ. Equation (14) may now be expressed as

$$\tilde{K_T} = \frac{K_T}{\kappa v_*(z + C_s\frac{v_*^2}{g})} = \left(\zeta\frac{\partial F_T}{\partial \zeta}\right)^{-1} \tag{16}$$

where C_s is an empirically-determined constant of the order of $10^4 - 10^5$. Because a typical value for h_s is $\sim 1\ m$, the direct influence of surface waves on ML structure is usually not important, but when h_s (or z_0) is introduced, it removes a singularity in the heat diffusion equation which occurs at $z = 0$. As a result, the solution becomes exact as the resolution is increased.

The stratification parameter S_p given in (13) may now be expressed in terms of the function F_T as

$$S_p = \kappa^{-2}\int_{\zeta_0}^{\zeta}(F_T(\zeta') - F_T(\zeta_0))\zeta' d\zeta'. \tag{17}$$

Equations (16) and (17) express implicitly the dependence of $\tilde{K_T}$ on the stratification parameter S_p.

[9] Note that the roughnes parameter below the sea surface differs from its counterpart in the atmospheric boundary layer since it now characterises not the typical height of roughness elementss but rather the entire depth of the subsurface layer which is mixed by breaking processes. Thus, we expect that z_0 below the sea surface should be considerably larger than it is in air.

The order of the moment included in the integral for S_p may be chosen arbitrarily. For convenience, we choose a simple definition for the stratification parameter which we define as the nondimensional integral density deficit (for $n = 0$),

$$S = \frac{\frac{g}{\rho_0}\int_{z_0}^{z}(\rho(z') - \rho(z_0))dz'}{v_*^2} \tag{18}$$

which is related to F_T by

$$S = \kappa^{-2}\int_{\zeta_0}^{\zeta}(F_T(\zeta') - F_T(\zeta_0))d\zeta' \tag{19}$$

The dependence of $\tilde{K_T}$ on S for stable stratification is obtained from Lettau's (1979) approximation for F_T and is shown in Fig. 6 (thin curve). We have chosen Lettau's results because they contain many cases of extremely stable stratification. For convenience in plotting, we use a transformed stratification parameter P instead of S, defined as

$$P = \begin{cases} log_{10}(1+S), & S \geq 0 \\ -log_{10}(1-S), & S < 0 \end{cases} \tag{20}$$

It is straightforward to determine the asymptotic behavior of the function $\tilde{K_T}(S)$ for free convection ($S \to -\infty$). This condition may occur for unstable stratification when $v_* \to 0$. In this case, K_T does not depend on v_* and $F(S) \propto S^{1/2}$. For stable stratification ($S > 0$), the situation becomes more complicated. Turbulence theory predicts that when $Ri > Ri_{cr}$, turbulence collapses and thus turbulent diffusion does not occur. In reality, however, finite heat fluxes, obtained by averaging over sufficiently long periods, do occur when $Ri > Ri_{cr}$, as confirmed by Lettau (1978). Thus, the function $K(P)$ does not approach zero even for large values of P.

The primary advantage of similarity theory in this case is that it does not require a priori knowledge of the mechanisms which produce the mixing. We have assumed that only the external forcing (characterized by v_*) and the stratification (which is expressed in terms of the integral density deficit) are important. For unstable stratification, mixing is produced mainly by the conversion of potential energy to the kinetic energy of turbulence. For neutral stratification, mixing exhibits the expected properties of a neutrally-stratified boundary layer. For stable stratification, the behavior of the turbulent mixing coefficient differs depending on the magnitude of the vertical

density gradient; it may increase with depth (for weak density gradients), but generally it decreases due to stratification. Approaching the upper thermocline, the turbulent mixing coefficient may decrease considerably but it still provides for at least limited mixing under conditions of strong stratification. If the ML becomes unstable, K_T may increase rapidly with depth, and then as the thermocline is approached, it decreases (Fig. 12). A similar situation arises in the atmospheric boundary layer when it is topped by an inversion.

The approach described above may appear oversimplified because it does not include any mechanisms for the propagation of kinetic energy or the supression of buoyancy effects. Mechanical energy which is transferred from the atmosphere to the ocean generates both surface waves and currents in approximately equal amounts (Chalikov, 1994). Vertical shear associated with the near- surface currents produces both turbulence and internal waves. The turbulence is partially dissipated through internal friction and mixing which increase the potential energy. Surface wave energy propagates over long distances, but is finally converted into (1) turbulence through wave dissipation, (2) currents (Chalikov and Belevich, 1994), and (3) internal waves. Vertical propagation of kinetic energy results from the stresses produced by currents and the diffusion of turbulent energy. For neutral stratification and steady-state conditions, the kinetic energy is eventually dissipated into heat. Under stratified conditions, a mutual exchange of turbulent and potential energies occurs. When the stratification is strongly stable, part of the mechanical energy derived from the wind goes into generating internal waves which are eventually converted into turbulence.

In summary, although all of the processes which contribute to mixing in the upper ocean are not known, we have assumed that the rate of mixing at each level depends only on the external momentum flux and the static stability of the layer above.

3. Application of the theory to temperature profiles acquired at OWSs PAPA, NOVEMBER and CHARLEY.

3.1 Data processing

In order to evaluate the function $\tilde{K}_T(P)$ which defines the nondimensional mixing coefficient, temperature profiles based on bathythermograph (BT) observations at OWS PAPA ($145°W$,$50°N$) for the years 1960-1967 were used. Each profile consists of 60 temperatures from the surface to a depth of 295 m, yelding a vertical resolution $\Delta z = 5\ m$. On average, the profiles were taken 3 hours apart. Occasionally there were gaps; one large gap of 77 days occurred during 1967. This interval was reconstructed using data from other years (via Fourier series expansion). After visual inspection, all profiles were interpolated to a uniform grid with a time step $\Delta t = 5.2$ hours, using a 4th-order β-spline interpolant (IMSL, 1991).

It is often difficult to compare one-dimensional models of the upper ocean with observed data. First, the data reflect not only local thermodynamic interactions with the atmosphere but also the effects of horizontal advection. Values for the advective term $c_w \rho_w U h \delta T / \Delta X$, even for weak currents ($U \simeq 0.1\ ms^{-1}$) and small horizontal temperature gradients ($\delta T / \Delta X \simeq 10^{-5}\ Km^{-1}$), often exceeds 200 Wm^{-2} for a layer depth of 50 m. Near ocean fronts, the divergence of horizontal heat advection may approach $10^4\ Wm^{-2}$, far greater than the expected heat exchange across the ocean surface itself. Thus, temperature variations due to local thermodynamic processes may often be obscured by the ffects of horizontal advection. A second source of error in estimating heat storage is due to the accuracy of the temperature measurements themselves ($\simeq 0.1\ K$).

The function $\tilde{K}_T(P)$ may be derived directly from the initial temperature profiles on the basis of the heat diffusion equation:

$$\frac{\partial T}{\partial t} = \frac{\partial}{\partial z} K_T \frac{\partial T}{\partial z} \tag{21}$$

From this equation the the heat diffusion coefficient may be obtained according to

$$K_T = \frac{H(z)}{\frac{\partial T}{\partial z}}, \tag{22}$$

where

$$\frac{H(t)}{c_w \rho_w} = \int_z^{h_a} \frac{\partial T}{\partial t} dz, \tag{23}$$

is the vertical heat flux and h_a is the depth of the active layer. It was assumed in deriving 22 and 23 that $H = 0$ at $z = h_a$.

Clearly, this method will often yield unacceptable results because it is based on finite differences where the observational noise is greatly amplified. To illustrate the magnitude of this problem, we estimate the possible error in heat flux by calculating the flux at the top of a unit water column with depth $\Delta z = 5\ m$ for a temperature chnge $\Delta T = 0.1\ K$ over a time interval $\Delta t = 5$ hours. Then

$$H = c_w \rho_w \frac{\Delta T}{\Delta t} \Delta z = 117\ Wm^{-2}. \tag{24}$$

This calculation shows that such errors can lead to fictitious heat fluxes which may exceed expected background levels. It also illustrates a major difference between atmospheric and oceanic boundary layers. If we assume that the vertical heat and momentum fluxes in air and water are of the same order, where the ratio of the vertical exchange coefficients in air (K_a) and water (K_w) is approximately equal to

$$v_{*w}/v_{*a} = \sqrt{\rho_a/\rho_w} \simeq 0.03, \tag{25}$$

and the ratio of the vertical temperature difference in water (ΔT_w) to air (ΔT_a) is $\sim 10^{-2}$, then the heat exchange in the ML may arise from very small temperature gradients which cannot be estimated accurately using routine oceanographic measurements. As a result, the ML appears to be homogeneous only because the specific heat capacity and the density are both large. In particular,

supercritical bulk Richardson numbers may, in fact, occur when the stratification appears to be neutral.

Clearly, the ML is mixed only to the extent that the vertical gradients which occur in this region are much smaller than those in the underlying thermocline. According to our previous estimate of the thermal time scales for the ML, temperature variations which originate at the surface propagate downward slowly so that instantaneous heat flux profiles in the ML are expected to be complicated functions of depth (Fig. 13). Finally, calculations of the vertical heat flux produced noise levels approaching values of $\pm 15,000 Wm^{-2}$! Thus, it was necessary to further pre-process the temperature profile data to reduce the noise to an acceptable level.

We have first attempted to reduce instrumental high-frequency noise by applying a Fourier transform to the time series of temperature at each level to obtain smooth estimates of $T(z)$, where

$$A^2(z,\omega) = \begin{cases} 0, & \text{if } F_{in}(z,\omega_c) - F_{in}(z,\omega) < (\delta T)^2/2, \\ A^2(z,\omega), & \text{otherwise,} \end{cases} \tag{26}$$

$A(z,\omega)$ is the amplitude of the Fourier transform of temperature at each level, ω is the radian frequency, and $F_{in}(z,\omega)$ is the integrated temperature spectrum defined as

$$F_{in}(z,\omega) = \int_0^{\omega} A^2(\omega,z)d\omega \tag{27}$$

where $\omega_c = 2\pi/\Delta t$ is the cut-off frequency and $\delta T = 0.1\ K$ is the instrumental error. This procedure removes the high-frequency fluctuations with dispersion $(\delta T)^2/2$, effectively smoothing the data. However, this procedure was not able to eliminate the fluctuations due to horizontal advection which occurred at considerably lower frequencies.

The seasonal evolution of the internal temperature field has been tracked by cross-correlating SST with the temperature at various levels below the surface. The resulting ensemble of cross-correlation functions is shown in Fig. 1. The correlations decrease and the phase shifts increase with increasing depth down to 150 m. Correlations below 150 m increase slightly and then decrease at deeper levels. The correlation structure below 150 m is evidently the result of larger-scale ocean-atmosphere interactions.

In pre-processing this data, we have assumed that the horizontal variability is coherent over depth. To suppress the fluctuations produced by

advection at depths $\geq 150\ m$, the following recursive algorithm was applied

$$A^2(z_i) = max(0, A^2(z_i) - \sum_{z_i < z \geq 150m} A^2(z_i)),\ i = n, n-1, ...1 \qquad (28)$$

where the amplitudes of the deeper fluctuations were extracted from Fourier spectra calculated at each level. [10]

Vertical profiles of the standard deviation of temperature obtained before and after applying (28) above are shown in Fig.2. As expected, the dispersion approaches zero at $z = 150\ m$. After excluding 'deep-water' modes from the spectra, the temperature variations in the upper layer became smooth enough to calculate reliable heat fluxes.

To check the effectiveness of the filtering procedure above, we compared the evolution of heat storage obtained by direct calculation of temperature averaged over depth, and through calculations of surface heat exchange.

The heat storage of the upper ocean can be estimated according to

$$Q_a(t) = H_a^{-1} \int_{H_a}^{0} T(t) dz, \qquad (29)$$

The results of this calculation are shown in Fig. 5 (upper frame).

An alternate method for the evaluation of Q_a consists of calculating a surface heat balance using meteorological observations. Unfortunately, significant errors also arise in estimating the various components of the surface heat balance. To calculate the sensible and latent heat fluxes and the friction velocities, four methods have been applied. The first method was similar to the scheme developed by Large and Pond (1981, 1982). The second method was based on nondimensional wind and temperature profiles obtained as semi-analytic solutions of the Mellor-Yamada Level 2 simplified turbulence closure scheme (Lobocki, 1993) together with the relationship for the thermal and dynamical roughness parameters derived by Liu et al. (1979). The third method, similar to the second, further assumed that the thermal and

[10] It was assumed that in the process of filtering, the phases of the remaining Fourier modes were left unchanged.

dynamical roughness parameters were essentially equal. The fourth scheme was based on the Businger-Dyer relationship for unstable conditions (Monin and Yaglom, 1971). For very stable conditions, it employs a correction for nondimensional wind and temperature profiles to account for the mixing associated with intermittent turbulent episodes. These four methods for calculating the heat fluxes gave results which differ by $\pm 20\ Wm^{-2}$. This range of uncertainty imposes a lower limit on the accuracy of estimating the surface fluxes by indirect methods. Because highly accurate data on surface heat fluxes are not available, we do not have a clear-cut basis for choosing any particular method. We have chosen (albeit somewhat arbitrarily), the third method which assumes that the dynamical and thermal roughness parameters are essentially equal. This method did, in fact, yield the smallest 8-year mean (residual) surface heat balance.

For calculating the incoming solar and long-wave radiation balance we have used an empirical method which relies on observed temperature and humidity and subjective estimates of total cloudiness (e.g., Martin, 1985). Precise calculations of the radiative fluxes are very sensitive to cloud amount and the associated properties of clouds. Thus, the results of indirect calculations often differ from actual measurements (e.g., Simpson and Paulson, 1979). This result has also been confirmed from radiation measurements acquired at OWS CHARLEY (Kazakov and Lukhachev, 1988). Differences between calculated and measured radiative fluxes are shown in Figs. 3 and 4. The large values of the shortwave and longwave radiation fluxes are clearly underestimated. These values in turn cause the amplitude of the annual variation in the surface heat balance to be underestimated.

The integral heat exchange, Q_a, has been calculated using meteorological observations over an 8-year period at OWS PAPA as follows,

$$Q_a(t) = \frac{1}{c_w \rho_w H_a} \int_0^t H(0) dt \tag{30}$$

Estimates of the integral heat exchange Q_a obtained from 29 and 30 are similar, but the amplitude of the annual variation in heat content is larger than the heat exchange itself (Fig 5, bottom panel). This discrepancy occurs because of inaccuracies in the heat balance calculations, and from incomplete removal of the contributions from horizontal advection. Nevertheless,

both methods give results which are in reasonable agreement. Note that the heat storage calculated from (29) using the unprocessed temperature data completely disagrees with the surface heat exchange, making it impossible to estimate $\tilde{K}_T$ with any reliability in this case.

Next, we use the pre- processed temperature data to estimate $\tilde{K}(S)$ which also requires salinity to calculate the stratification parameter. Because salinity data were not available at OWS PAPA, the annual salinity cycle was taken from the monthly-averaged salinity profiles of Tabata and Peart (1985). These data were interpolated to the previous 5 m vertical temperature grid and expanded in a Fourier series to estimate the instantaneous values of salinity. Extinction of the incoming solar radiation was then calculated for type II waters according to Jerlov (1976).

3.2 Evaluation of $\tilde{K}_T$

The analytic form of $\tilde{K}_T(S)$ was obtained by direct solution of the heat diffusion equation,

$$\frac{\partial T}{\partial t} = \frac{\partial}{\partial z} K_T \frac{\partial T}{\partial z} + \frac{\partial F_s}{\partial z} \tag{31}$$

where F_s is the solar heat flux. It was assumed that

$$K_T \frac{\partial T}{\partial z} + F_s = H, \qquad at\ z = 0$$
$$K_T \frac{\partial T}{\partial z} + F_s = 0, \quad at\ z = 300\ m$$

This method relies on the high heat capacity of the ocean and, thus, significantly reduces the influence of noise. It minimizes the *rms* difference between the observed and simulated temperature profiles through successive corrections to $\tilde{K}$. Since this function has many degrees-of-freedom, we restrict its form by the use of a simple approximation. Using the results of Lettau (1979) as a first-guess (Fig. 6), the following three-parameter formula

has been chosen to accomplish this,

$$\tilde{K}_T = \begin{cases} (1 - \lambda S)^{0.5}, & \text{if } S < 0 \\ (1 + \alpha S)^{-\beta}, & \text{if } S > 0 \end{cases} \tag{32}$$

where α, β and λ are estimated from the of data.

Equation (31) was solved semi-implicitly, using the turbulent mixing coefficient obtained from the previous time step. This scheme permitted us to choose a time step that corresponded to the time interval between the processed profiles. The first temperature profile was used to establish the initial conditions. The integration was performed for time steps of $\Delta t = 5.2$ hours for N=13,340 steps.

To evaluate the results, vertical profiles of the bias and rms differences were calculated between the simulated and observed temperatures where

$$\Delta T_{bias} = \frac{1}{N} \sum_{1}^{N} (T_{calc} - T_{obs}) \tag{33}$$

$$\Delta T_{rms} = \left(\frac{1}{N} \sum_{1}^{N} (T_{calc} - T_{obs})^2 \right)^{1/2} \tag{34}$$

The largest rms error ($\delta T = max(\Delta T_{rms})$) that occurred over depth was used as an objective criterion for accuracy. Smaller values of δT in the vicinity of 1 K were concentrated along the curve in (α, β) space. A minimum δT of 0.83 K occurred at $\alpha = 5.0$, $\beta = 1.80$. As a result, the nondimensional function $\tilde{K}_T(S)$ assumed the following form (Fig. 6, thick line)

$$\tilde{K}_T = \begin{cases} (1 - 0.8S)^{0.5}, & \text{if } S < 0 \\ (1 + 5.0S)^{-1.8}, & \text{if } S > 0 \end{cases} \tag{35}$$

The results were insensitive to the value of λ chosen over the range $0.01 < \lambda < 1.5$. Thus, we conclude that for unstable stratification, the turbulent mixing coefficient should be large enough to produce homogeneity, but that its precise value is not important. Consequently, we have chosen $\lambda = 0.8$, taken from Lettau (1979). However, the results are very sensitive to the functional form of $\tilde{K}_T(S)$ for $0 < S < 10^4$, the interval which is responsible for the formation of the upper thermocline.

3.3 Simulations at OWS PAPA

The data used to evaluate the two numerical constants in (32) were next used to simulate the 8-year evolution of the upper ocean at OWS PAPA ($145°W$,$50°N$). Vertical profiles of ΔT_{bias} and ΔT_{rms} between observed and simulated temperatures at OWS PAPA indicate that the maximum bias does not exceed 0.5 K and the maximum rms does not exceed 1 K (Fig. 7). The observed and simulated temperatures at depths of $0 - 60$ m are displayed in Fig. 8. The observed data are still somewhat noisy after filtering, but the simulated variations in temperature (in response to surface forcing) are generally in good agreement with the observations. Sequences of observed (filtered) and simulated profiles for the year 1966 with intervals of about 3 days between profiles are displayed in Figs. 9 and 10, respectively. Although the observed and simulated profiles are generally similar, many of the details in the observed profiles are not reproduced. Such discrepancies may be due to the residual influences of horizontal and vertical advection. Vertical profiles of the stratification parameter P, and the turbulent mixing coefficient K_T, are shown in Figs. 11 and 12 where the upper layer was always assumed to be well-mixed. Negative values of P (and S) correspond to periods of convection where the turbulent mixing coefficient produces a homogeneous ML, particularly during the fall and winter. Approaching the thermocline, the stratification becomes stable, but the turbulent mixing coefficient is still large enough to produce extensive turbulent entrainment. This smooth transition from moderate to very stable stratification occurs because of our appropriate choice of the integral stratification parameter.

In summer, the upper ocean is generally stable, but isolated episodes of convection produced by transient atmospheric disturbances or diurnal cooling may occur. The vertical heat flux profiles shown in Fig. 13 exhibits irregular behavior with large fluxes occurring sporadically throughout the sequence. This 'intermittence' was produced partly by truncation effects which caused large gradients to migrate abruptly from one layer to the next. Additional calculations using increased vertical resolution show that these large, intermittent vertical fluxes occur more frequently but with decreased amplitudes.The primary reason for these fluctuations is due to the sharp increases in wind forcing or surface cooling which cause the upper thermocline to retreat, often followed by periods of transient heat fluxes. Additional cal-

culations confirm that these heat fluxes do, upon occasion, greatly exceed the surface heat fluxes. Thus, the heat that enters the ocean across its surface is initially stored in the ML, and the large heat fluxes within the ocean interior occur only infrequently.

Because $\tilde{K}_T(S)$ was derived for the specific conditions at OWS PAPA, its applicability to other oceanic regions was initially open to question. To examine this issue, we subsequently apply this model to other oceanic regions.

3.4 Simulations at OWS CHARLEY

The temperature and salinity data for OWS CHARLEY ($53°N$, $35°W$) contain hourly profiles at standard depths down to $z = 500\ m$ and meteorological data which include direct observations of shortwave and longwave radiation (Kazakov and Lukhachev, 1988) for a period of one year. A comparison of the observed and calculated radiation balance is shown in Figs. 3 and 4. Missing data were reproduced using the same method that was used in processing the data from PAPA. Vertical profiles of the bias and the *rms* differences between the observed and simulated temperatures are shown in Fig. 14. The ratio of the *rms* SST to the *rms* temperature at 300 m is approximately equal to 6, thus, most of the anuual variability is produced by local interactions with the atmosphere. A comparison of the initially-unprocessed and the simulated evolution of the thermal structure at OWS CHARLEY for different depths shows that our model reproduces the annual variation of temperature reasonably well (Fig. 15).

3.5 Simulations at OWS NOVEMBER

To further validate our results from PAPA, we used 10 years of data (1960 to 1970) from OWS NOVEMBER ($30°N$, $140°W$). This station is located in a region of variable thermal structure due, in part, to its close proximity to the Subtropical Front in the northeast Pacific (Tomczak and Godfrey, 1994). A standard deviation of temperature at NOVEMBER is given by curve 3 in Fig 16. As seen, an annual variability of temperature at NOVEMBER is very large up to depth 300 m. A static stability below $100 - 150\ m$ is very high during entire year, thus, much of the variability at NOVEMBER may not be

due to local forcing and it becomes more difficult to compare the observed and simulated data in this case. Nevertheless, we have proceeded to explore the applicability of the function $\tilde{K}_T$, derived from PAPA data, to simulate the 10-year evolution of vertical temperature structure at NOVEMBER. These data consist of 10206 temperature profiles which have been interpolated to a regular, 5 m vertical grid. Again, the data were noisy, irregularly spaced in time, and gappy, but on this occasion we were not able to interpolate these data successfully using Fourier techniques and a comparison calculated data were made with unfiltrated observational data. Vertical profiles of ΔT_{bias} and ΔT_{rms} between observed and simulated temperatures at OWS NOVEMBER indicate that the maximum bias does not exceed 0.7 K and the maximum rms does not exceed 1.5 K (Fig. 16). The observed and simulated temperatures at depths of $0 - 120$ m are displayed in Fig. 17. The observed data are very noisy, but the simulated variations in temperature are in reasonable agreement with the observations.

4. Cases of idealized forcing

Following our previous discussion, the evolution of the thermohaline structure of the upper ocean may be described by the heat diffusion equation (31) and the following equation for salinity diffusion

$$\frac{\partial s}{\partial t} = \frac{\partial}{\partial z} K_s \frac{\partial s}{\partial z}. \tag{36}$$

The boundary conditions at $z = 0$ are $K\frac{\partial T}{\partial z} = H/(c_w \rho_w)$ and $K\frac{\partial s}{\partial z} = G$, where H and G are the surface fluxes of heat and salt, respectively. In the following analysis, we use a linearized equation of state for sea water $\rho' = \alpha T' + \beta s'$ (where ρ', T' and s' are perturbations of density, temperature and salinity, respectively, $\alpha = \frac{\partial \rho}{\partial T}$ and $\beta = \frac{\partial \rho}{\partial s}$,). Incoming solar radiation is not included here. We also assume that $K_T = K_s$. Next, we introduce the equation of density diffusion, forced by the surface mass flux $M = \alpha c_w^{-1} H + \rho_w \beta G$.

4.1 Constant heating and cooling

First, we consider the case where an initially stratified liquid with a constant density gradient $\partial\rho/\partial z > 0$ (for the z axis pointing downward), is modified under the action of a constant surface stress τ_0, and a constant surface heat flux, H_0. For convenience, we use the water friction velocity $v_* = \sqrt{\tau/\rho_w}$ instead of τ. Using the buoyancy parameter g/ρ_0, we now introduce the Monin-Obukhov length (L) and density (ρ_*) scales and a time scale t_*, where

$$L = \frac{\rho_0 v_*^3}{gM}, \quad \rho_* = \frac{M}{v_*}, \quad t_* = \frac{L}{v_*} \tag{37}$$

A dimensionless equation for density diffusion is obtained, where

$$\frac{\partial\tilde{\rho}}{\partial\tilde{t}} = \frac{\partial}{\partial\tilde{z}}\tilde{K}\frac{\partial\tilde{\rho}}{\partial\tilde{z}} \tag{38}$$

where the tilde ($\sim$) indicates the nondimensional variables. At $\tilde{z} = 0$ the nondimensional density flux $\tilde{K}\frac{\partial\tilde{\rho}}{\partial\tilde{z}}$ is equal to 1 and the initial condition becomes $\tilde{\rho} = \gamma\tilde{z}$. Thus, the solution depends only on one parameter, the initial density gradient, $\gamma = \partial\tilde{\rho}/\partial\tilde{z}$.

The evolution of the ML depth (depth of the maximum density gradient) under conditions of surface heating and initially neutral stratification ($\gamma = 0$) has been calculated (Fig. 18, Curve 1). The remaining curves in Fig. 18 have been calculated for several density gradients under conditions of cooling (positive surface mass flux). The ML depth is shallow under these conditions. A sequence of nondimensional density, stratification, turbulent mixing coefficient, and heat flux profiles for initially neutral stratification is displayed in Fig. 19. A positive density flux occurs only at the top of the ML. A much larger negative density flux occurs near the bottom of the ML due to mixing in the upper thermocline. The evolution of nondimensional density, stratification, turbulent mixing coefficient, and heat flux profiles for this regime is displayed in Fig. 20.

Profiles for unstable stratification show that the ML is more homogeneous and much deeper than it was for the case of heating. Most of the ML participates in the convection in this case when the stratification parameter S

is negative. Also, the surface density flux, although small in absolute value, is positive compared with the negative heat flux that occurs in the upper thermocline. Thus, cooling of the ML during the fall occurs through the turbulent entrainment of cold water, producing a ML which deepens with time.

4.2 Wind mixing

Next, we consider the evolution of an initially stratified upper ocean with an initial density gradient $\gamma = \partial\tilde{\rho}/\partial\tilde{z}$, forced by a wind stress which is characterized by the water friction velocity v_*. Scales for the length L', density ρ'_*, and time t'_* now take the form

$$L' = \left(\frac{1}{\rho_0}\frac{\partial\rho}{\partial z}\right)^{-1}, \quad \rho'_* = \rho_0, \quad t'_* = \left(\frac{v_*}{\rho_0}\frac{\partial\rho}{\partial z}\right)^{-1} \tag{39}$$

At $\tilde{z} = 0$, the nondimensional density flux is equal to 0 and the initial condition becomes $\tilde{\rho} = 1 + \tilde{z}$. Evolution of the density structure for the upper layer for pure wind mixing is shown in Fig. 21. This case is similar to the case for surface cooling, but is less intense because of the stratification.

4.3 *Free convection*

The present scheme does not account for free convection above a stratified layer, although (35) has the correct asymptotic form. Unstable stratification occurs at the top of the ML, but stable stratification occurs below (Fig. 11). In this case, when $v_* = 0$, the stratification parameter S is not defined. However, this condition is not critical for the parameterization of mixing because the wind speed is rarely equal to zero, plus the results are not strongly dependent on this value in any case. However, this scheme can be extended to include free convection. In this case, for $M < 0$, the friction velocity can be replaced by the sum of the friction velocity and the convective velocity scales (e.g., Beljaards, 1994), where the convective velocity scale w_* is

$$w_* = \alpha_c \left(-\frac{g}{\rho_0} M h_m\right)^{1/3} \tag{40}$$

By replacing the friction velocity by the sum of the friction velocity and the

convective velocity scale, we obtain

$$K_T = \kappa(v_*^2 + w_*^2)^{1/2} z F(S') \tag{41}$$

and

$$S' = \frac{\frac{g}{\rho_0}\int_{z_0}^{z}(\rho(z') - \rho(z))dz'}{v_*^2 + w_*^2} \tag{42}$$

where h_m is the depth of the ML and α_c is an empirical constant, which, according to data obtained in the ASL, is close to unity (Monin and Yaglom, 1971).

4.4 Diffusion of momentum.

The only dynamical parameter needed to reproduce the evolution of the thermohaline structure of the upper ocean is the surface wind stress. An important additional characteristic of the upper ocean is the vertical distribution of currents. To calculate current profiles, it is necessary to estimate the value of the momentum exchange coefficient, K_M. According to Monin-Obukhov similarity theory, the turbulent Prandtl number $Pr = K_M/K_T$ is a function of the nondimensional vertical coordinate $\zeta = z/L$. As was seen earlier, ζ is related to the nonlocal stratification parameter S, so that Pr may be expressed as a function of S. This dependence has been calculated using Lettau's (1979) data to obtain the following approximate relation for Pr,

$$log_{10}Pr = \begin{cases} -0.67 + 0.1383P, & if\ P < -0.6, \\ 0.364P + 0.165P^2 - 0.082P^3 - 0.0770P^4, & if\ -0.6 \leq P \leq 0.8, \\ 0.079 + 0.3017P, & if\ P > 0.8, \end{cases} \tag{43}$$

where P is the transformed stratification parameter given in (20). Relation (43) assumes that K_M is slightly less than K_T for unstable stratification, but may be several times larger than K_T for stable stratification.

4.5 Mixing at deeper levels

Mixing in the ocean interior below the seasonal thermocline (150-300m) is poorly understood. However, it may be taken into account using a constant

(residual) value for the mixing coefficient. This mixing, although less intense than mixing near the surface, is responsible for interannual variability of the thermal structure below the seasonally active ocean layer.

5. Related topics

5.1 The influence of vertical resolution

The temperature profiles observed at OWS's PAPA, CHARLEY and NO- VEMBER were simulated using a uniform vertical grid with spacing of $\Delta z = 5\ m$. A temperature diffusion equation identical to (8) was solved using a semi-implicit scheme where the turbulent mixing coefficient was taken from the previous time step. The time steps were varied from 1 to 5 hours. The results were not sensitive to the choice of time step.

A model simulation was performed on a nonuniform vertical grid for a layer depth h_a and stretched according to a logarithmic transformation. In most models of the upper ocean, the turbulent mixing coefficient decreases rapidly with depth. This property leads to the formation of high gradients in the upper thermocline. In our scheme, the turbulent mixing coefficient profile tends to be smoother than it is in models which are based on closure schemes. We have examined the possibility that the occurrence of large vertical gradients of the turbulent mixing coefficient may cause various models to become highly sensitive to the choice of vertical resolution. To illustrate this effect, we performed a series of model simulations for idealized annual forcing for different vertical resolutions for the upper 200m. In this layer, a vertical resolution of 1 m was initially adopted. The results obtained using this resolution were accepted as the 'exact' solution. The deviations that occurred when lower resolutions were used are presented in Figs. 22 and 23. The dependence of these results on vertical resolution was unexpectedly large. For typical resolutions in the upper layer of the order of $20m$, the rms differences in some cases exceeded 1 K, compared to the 'exact' solution. It is likely that better results may be obtained by an appropriate modification

of $\tilde{K}_T(S)$. This function is a model-specific construct and should be chosen and tuned with empirical data for the particular vertical resolution chosen.

5.2 Assimilation of sea surface temperature (SST) and its predictability

We have investigated several simple schemes for vertical assimilation, where the observed SSTs were assimilated using unit weighting. An observed temperature profile was used to generate the necessary initial conditions. Any assimilation procedure that blends observed SSTs into model-generated fields must take into account the vertical structure of the upper ocean. The best results were obtained with the following scheme for extrapolating the observed surface temperature $T_o(0)$ to subsurface levels

$$T_a(z) = \begin{cases} T_s(h_m) + (T_o(0) - T_s(h_m))\frac{\rho(z)-\rho(h_m)}{\rho(0)-\rho(h_m)}, & \text{if } T_o(0) > T_s(0) \\ min(T_s(z), T_o(0)), & \text{otherwise} \end{cases} \tag{44}$$

where T_s is the temperature before, and T_a the temperature after, assimilation, and h_m is the ML depth defined as before. Assimilation of the observed SST, $T_o(0)$, is different for cases when the observed SST is larger than the simulated (i.e., model-derived) T_s, and vice versa. When the observed SST exceeds the simulated SST, the difference $T_o(0) - T_s(h_m)$ is distributed over the depth of the ML proportional to the nondimensional density profile (e.g., normalized by the difference $\rho(0) - \rho(H_m)$). When the observed SST is lower than the simulated value, the temperature $T_o(0)$ replaces the simulated temperature $T_s(z)$ to the depth where they become equal. Our results show that this approach does not destroy the previous vertical structure of the upper ocean.

This algorithm was used to assimilate SSTs in the simulations of temperature evolution at OWS PAPA. Significant error reduction occurred for predicted temperatures at the top of the ML ($z < 50\ m$); below the ML, the errors increased slightly (Fig. 24). These results were then used to calculate correlations between the observed and simulated SST and temperature at lower levels. By removing seasonal effects (Fig. 1), we calculated the correlations of the temperature deviations from the annual mean (i.e., anomaly correlations), averaged over an 8-year period. The results are shown in Fig.

25. Hindcasted SSTs also produced relatively high levels of predictability. Contrary to our initial expectations, however, more frequent assimilation of SSTs did not improve the agreement between the simulated and observed profiles significantly. Finally, for hindcasts produced over longer time periods, the correlations remained statistically significant (0.6-0.7). A predictability of temperature at deeper levels is significantly lower, because there was not assimilation.

The results obtained on the sensitivity of the simulation of the temperature profiles to the choice of vertical resolution and on SST data assimilation, are preliminary but suggest that additional work is needed in these areas.

6. Concluding remarks

Many mechanisms contribute to the vertical heat and mass exchange in the upper ocean. Consequently, it is difficult to parameterize such phenomena on a purely theoretical basis. We have developed a new approach for predicting the evolution of the upper ocean under the action of variable forcing using observational data. This approach is based on a modification of Monin-Obukhov similarity theory for stratified boundary layers. This theory has been reformulated to account for the large thermohaline inertia of the upper ocean. It has been assumed that the dynamical structure of the upper ocean is primarily influenced by the mean surface forcing. The vertical density structure is characterized by a stratification parameter which takes into account the density deficit (or potential energy) as a function of depth. Observed temperature profiles were used to determine the appropriate scaling and a nondimensional turbulent mixing coefficient as a function of the stratification parameter. This approach is not restricted to the mixed layer, but includes the upper thermocline as well. As a result, it may be used to simulate short-term fluctuations plus the seasonal and interannual variability of the upper ocean.

The above scheme is based on the governing diffusion equations for temperature, salinity and momentum which include the turbulent mixing coefficients for heat, and momentum exchange; these coefficients, in turn, depend

on a predefined stratification parameter. This approach has been validated by simulating the evolution of the upper ocean in three widely separated oceanic regions. Overall, the results of these simulations confirm that this simple scheme for turbulent mixing is able to reproduce the annual evolution of the upper ocean and smaller-scale perturbations due to weather- related synoptic disturbances rather well. It has also yielded results which are equivalent to those obtained using more complicated turbulent closure models (e.g. Martin, 1985, Kantha and Clayson, 1995). Our approach, because of its mathematical simplicity, computational efficiency, and reasonable accuracy is well-suited for implementation in large- and mesoscale ocean models.

One limitation of the approach given here is that it is strictly valid only for an ocean boundary layer forced by local interactions with the atmosphere. Upon occasion, however, turbulence may be created in regions where large gradients are produced by baroclinic currents. Clearly, when turbulence is generated in this manner, our scheme will underestimate the intensity of vertical mixing.

Assimilation of SST data based on modified temperature profiles for the upper ocean showed considerable improvement for SST hindcasts, for relatively low rates of assimilation (once per month). If assimilation is performed more frequently, it was found that the data may not always be consistent with model output. This problem may be reduced by further adjustments to the derived nondimensional turbulent mixing coefficient, $K_T(S)$.

The results of simulating thermal structure in the mixed layer and the upper thermocline are particularly sensitive to vertical resolution. However, this problem is inherent to any model which employs a variable turbulent mixing coefficient. It is very possible that the derived function $K_T(S)$ will not produce optimum results if it is implemented directly in models with low vertical resolution. However, it should be possible to apply this function to a modified vertical grid with increased resolution or to use a nested vertical grid to obtain satisfactory results.

Acknowledgements

The authors wish to thank Dr. P. Martin for the data from OWSs PAPA and NOVEMBER, Dr. V. Kuzin for the data from OWS CHARLEY. The authors would also like to thank Dr. D.Sheinin for helpful discussions and Drs. D.B. Rao, P. Long and G. Mellor for reviewing the manuscript and making many valuable comments.

References

Beljaards,A.C.M. 1994: The parameterization of surface fluxes in large-scale models under free convection *Q. J. R. Meteorol. Soc.*, **121**, 255-270.

Bryan, K.,1963: A numerical investigation of a nonlinear model of a wind-driven ocean. *J. Amos. Sci.*, **20**, 594-606.

Bryan, F., 1987: Parameter sensivity of primitive equation ocean circulation models. *J. Phys. Oceanogr.*, **17**, 1279,1287.

Chalikov, D., 1995: The Parameterization of the Wave Boundary Layer. *J. Phys. Oceanogr.*, **25**, 1335-1349.

Chalikov, D., and M.Belevich 1994: One-dimensional theory of the wave boundary layer. *Boundary-Layer Met.* **63**, 65-96.

Charnock, H., 1955: Wind stress on a water surface. *Quart. J. Roy. Meteorol. Soc.*, **81**, 639.

Cox, M.D. 1975:A baroclinic numerical model of the world ocean: preliminary results. *Numerical Models of Ocean Circulation*, Nat. Acad. of Sciences. Washington D.C., 107-120.

Gregg, M.C. 1987: Diapycnal Mixing in the Thermocline: A Review. *J. Geophys. res.*, **92**, 5249-5286.

Jerlov, N.G., Marine optics. Elsevier, New-York, 1976.

Kantha L.H. and C.A. Clayson: 1995 An improved mixed layer model for geophysical applications. *J. Geophys. Res.*, **99,**, 25,235-25,266.

Kazakov, A.,L. and S.M. Lukhachev 1988: Specialized archive of observation data for the atmosphere-ocean interaction modeling. In: Mathematical models inocean dynamics investigation. Novosibirsk, 82-95.

Kitaigorodskii. S.A. 1970: The Physics of Air-Sea interaction. Gidrometeoizdat, Leningrad, 284 pp. (In Russian. English translation: Israel Progr. Sci. Translation, Jerusalem, 1973, 236 pp).

Kraus, E and J. Turner, 1967: A one-dimensional model of the seasonal thermocline. Pt II: The general theory and its consequences. *Tellus*, **19**, 98-106.

Large, W.G., J.C. McWilliams, and S.C. Doney, 1994: Oceanic vertical mixing: a review and a model with a nonlocal boundary layer parameterization. *Reviews of Geophysics*, **32**, 4, 363-403.

Lettau H.H.: 1979, Wind and temperature profile function for diabatic surface layers including strong inversion cases. *Boundary Layer Meteor.* **17** 443-464.

Lineykin, P.S. Main problems of dynamic theory of the ocean baroclynic layer. 1957, Gidrometeoizdat, 139 pp.

Lobocki, L., 1993: A Procedure for the derivation of Surface-Layer Bulk Relationships from simplified Second-Order Closure Models. *J. Appl. Met.*, **32**, 126-138.

Martin P.J. 1985: Simulation of the Mixed Layer at OWS November and Papa With Several Models. *J. Phys. Oceanogr.*, **90**, 903-916.

Mellor, G. and T. Yamada, 1974 A hierarchy of turbulent closure models for planetary boundary layers. *J. Atmos. Sci.*, **31**, 1791-1806.

Mellor, G. and T.Yamada, 1982: Development of turbulence closure model for geophysical fluid problems. *Rev. Geophys. Space Phys.*, **20**(4), 851-875.

Monin A.S. and A.M. Obukhov, 1954: Basic Laws of Turbulent Mixing in the atmosphere near the Ground. *Tr. Acad. Nauk SSSR, Geofiz. Inst.* No. 24,(151), 163-187.

Monin A.S. and A.M.Yaglom, 1971: Statistical fluid mechanics. The MIT Press. 769 pp.

Muller P., 1993: Diapycnal Mixing in the Ocean: A Review. In: Large eddy simulation of complex engineering and geophysical flows., Cambridge Univ. Press., 455-487.

Munk, W. and J. Anderson 1948: Notes on a theory of the thermocline. *J. Mar. Res.*, **7**, 276-295.

Obukhov A.,M. 1946: Turbulence in thermally inhomogeneous atmosphere. *Trudy Ins. Teoret. Geofiz. AN SSSR*, No.24(151),95-115.

Simpson J.J. and C.A. Paulson (1979) Mid-ocean observation of atmospheric radiation. *Quart.,J.,R., Met., Soc.*, **105**, 487-502.

Tabata, S. and J.L. Peart 1985: Statistics of Oceanographic Data Based on Hydrographic/STD Casts Made at Ocean Station R During August 1956 through June 1981. *Canadian Data Report of Hydrography and Ocean Sciences*, No. 31. 97 pp.

Tolman H.L. and D. Chalikov, 1995: On the source terms in a third-generation wind wave model. Submitted to *J. Phys. Oceanogr.*

Tomczak, M., and J.S. Godfrey, 1994: Regional Oceanography: An Introduction. Elsevier Science Inc., Tarrytown, New York, 444 pp.

Troen, I.B., and L. Mahrt, 1986: A simple model of the atmospheric boundary layer; Sensivity to surface evaporation,*Boundary Layer Meteorol.*, **37**, 129-148.

Figure captions

Fig.1 Cross-correlation of SST with temperature at different levels (the depths (m) are shown in the legend).

Fig. 2 Vertical profiles of observed temperature standard deviation: 1 - before processing; 2 - after reduction of the noise and fluctuations produced by advection.

Fig. 3 Dependence of difference between calculated and measured surface shortwave radiation fluxes at OWS CHARLEY relative to the measured values. Vertical bars denote variability, dotted line is the number of cases (right axis).

Fig. 4 The same as in Fig. 3, but for longwave radiation.

Fig. 5 Temporal evolution of heat storage (formula (29)) and integrated surface heat balance (formula 30) for OWS PAPA. For easy comparison curve calculated with Eq. 29 is shifted vertically to constant $Q_a(0)$.

Fig. 6. Dependence of nondimensional turbulent mixing coefficient $\tilde{K}_T = K_T/(\kappa v_* z)$ on the stratification parameter P for stable stratification. The thin curve is calculated using Lettau's (1979) approximation obtained for a stable atmospheric surface layer. The solid curve was obtained by minimizing the deviations between the observed and simulated temperature profiles for OWS PAPA.

Fig. 7 Vertical profiles of bias ΔT (curve 1), $\Delta T_{rms}(C)$ difference between observed and calculated temperatures (curve 2), and dispersion of observed temperature (curve 3) for 1960-1967 at OWS PAPA.

Fig. 8 Observed and simulated evolution of temperature at different levels for OWS PAPA.

Fig. 9 Sequence of observed temperature profiles $T(z)(C)$ for 1966 year with a time interval of approximately 3 days.

Fig. 10. Similar to Fig. 9 but for simulated temperature profiles $T(z)(C)$.

Fig. 11. Similar to Fig. 9 but for the nondimensional stratification parameter P (formula 20).

Fig. 12. Similar Fig. 9 but for $log_{10}(K(m^2c^{-1}))$.

Fig. 13. Similar Fig 9 but for transformated vertical heat flux $\hat{H}$, where

$$\hat{P} = \begin{cases} log_{10}(1 + H(Wm^{-2})), & H \geq 0 \\ -log_{10}(1 - H(Wm^{-2})), & H < 0 \end{cases} \tag{45}$$

Fig. 14. Bias (curve 1), *rms* difference (C) between simulated and observed temperatures for OWS CHARLEY (curve 2), standard deviation of observed temperature (curve 3) for 1 year.

Fig. 15. Observed and simulated annual evolution of temperature at different levels for OWS CHARLEY.

Fig. 16. Bias (curve 1), *rms* difference between simulated and observed temperature deviation from T(z=200m) for OWS NOVEMBER (curve 2), Dispersion of observed (curve 3) and measured temperature deviation from $T(z = 200m)$ (curve 4) for 10-year period.

Fig 17. Observed and simulated evolution of temperature deviation from$T(z = 200m)$ at different levels for OWS NOVEMBER.

Fig. 18. Evolution of nondimensional mixed layer depth $\tilde{h} = h/L$ for constant forcing. Curve 1: $10\tilde{h}$, negative mass flux, initial density gradient $\gamma = 0$. Curves 2-10 - positive mass flux: curve 2 -*gamma* = 100, 3 - $\gamma = 200$, 4 - $\gamma = 300$, 5 - $\gamma = 400$, 6 - $\gamma = 500$, 7 - $\gamma = 600$, 8 - $\gamma = 700$, 9 - $\gamma = 800$, 10 - $\gamma = 900$, 11 - $\gamma = 1000$.

Fig. 19. Sequence of nondimensional density , stratification, turbulent mixing coefficient and density flux profiles with a nondimensional time interval $\tilde{t} = 1000$ for initially neutral stratification and negative mass flux.

Fig. 20. Sequence of nondimensional density , stratification, turbulent mixing coefficient and density flux profiles with nondimensional time interval $\Delta\tilde{t} = 1000$ for $\gamma = 100$.

Fig. 21. Sequence of nondimensional density , stratification, turbulent mixing coefficient and density flux profiles with nondimensional time interval $\tilde{t} = 1000$ for pure wind forcing and an initially stably stratified ocean.

Fig. 22. Effect of vertical resolution for model annual forcing simulated for a logarithmically stretched vertical grid. Solid line 1 represents the annual dispersion for the 'exact' solution (top axis). Left-hand curves (top axis) show rms difference and the middle curves (bootom axis) show the bias between the 'exact' solution (with 200 points in a layer $0 - 200m$ thick and an upper vertical step $\Delta z_1 = 0.02\ m$) and solutions for : $2 - L = 79, \Delta z_1 = 2\ m$, $3 - L = 46, \Delta z_1 = 4\ m$, $4 - L = 32, \Delta z_1 = 6\ m$, $5 - L = 24, \Delta z_1 = 8\ m$, $6 - L = 19, \Delta z_1 = 10\ m$, $7 - L = 16, \Delta z_1 = 12\ m$, $8 - L = 14, \Delta z_1 = 14\ m$, $9 - L = 12, \Delta z_1 = 16\ m$, $10 - L = 11, \Delta z_1 = 18\ m$, $11 - L = 11, \Delta z_1 = 20\ m$.

Fig. 23. Annual evolution of SST simulated with model forcing for different vertical resolutions (see caption to Fig. 22).

Fig 24. Effect of SST data assimilation once per month. The vertical profiles of bias ΔT (curve 1), rms ΔT_{rms} difference between observed and calculated temperature (curve 2) and dispersion of observed temperature (filtered)(curve 3)obtained by simulating 8 years of data at OWS PAPA. Compare with results without data assimilation in Fig. 7.

Fig. 25. Correlation observed and simulated temperature anomalies at different depths for OWS PAPA calculated over an ensemble of 96 consecutive month at w/s PAPA after SST monthly assimilation.

Fig.1

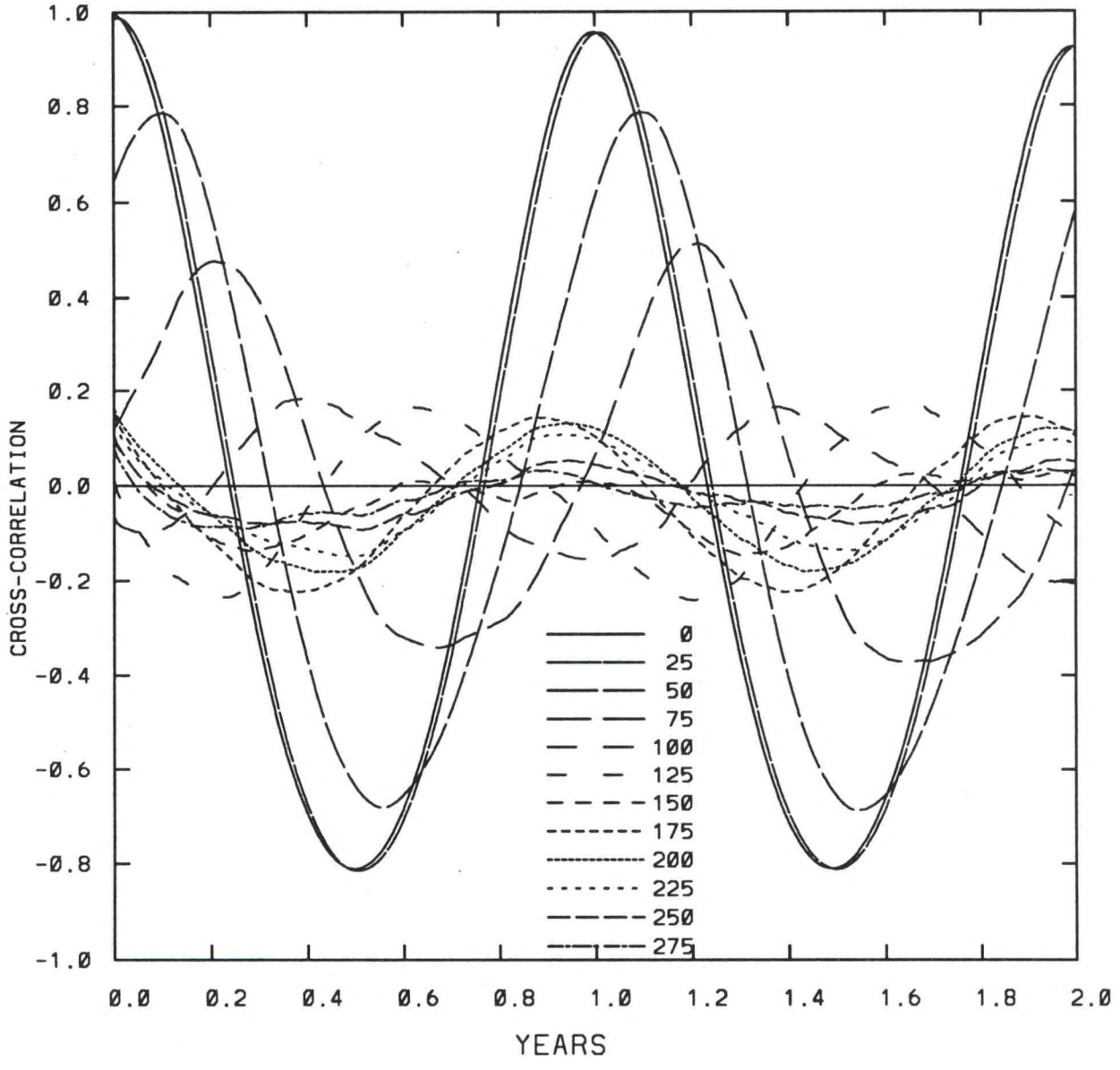
1.0
0.8
0.6
0.4
0.2
0.0
-0.2
-0.4
-0.6
-0.8
-1.0
CROSS-CORRELATION
0.0
0.2
0.4
0.6
0.8
1.0
1.2
1.4
1.6
1.8
2.0
YEARS
0
25
50
75
100
125
150
175
200
225
250
275

Fig.2

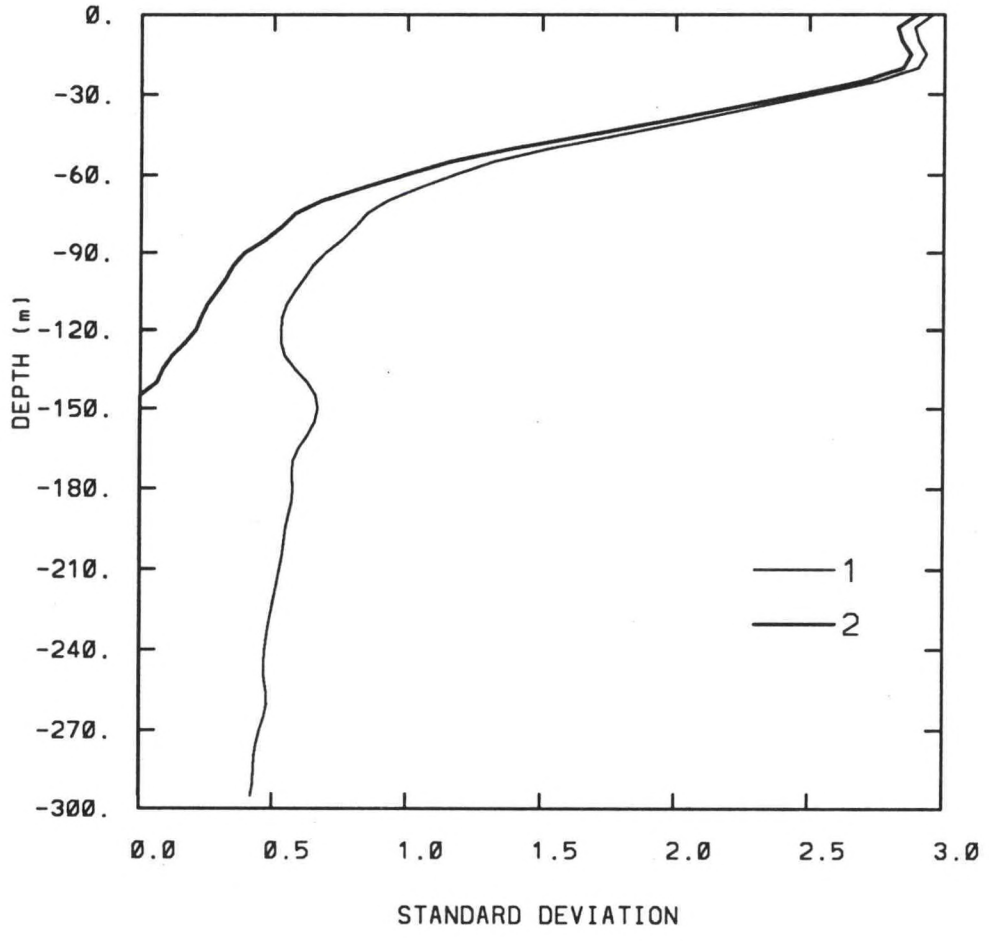
0.
-30.
-60.
-90.
-120.
-150.
-180.
-210.
-240.
-270.
-300.
DEPTH (m)
0.0
0.5
1.0
1.5
2.0
2.5
3.0
STANDARD DEVIATION
1
2

Fig. 3

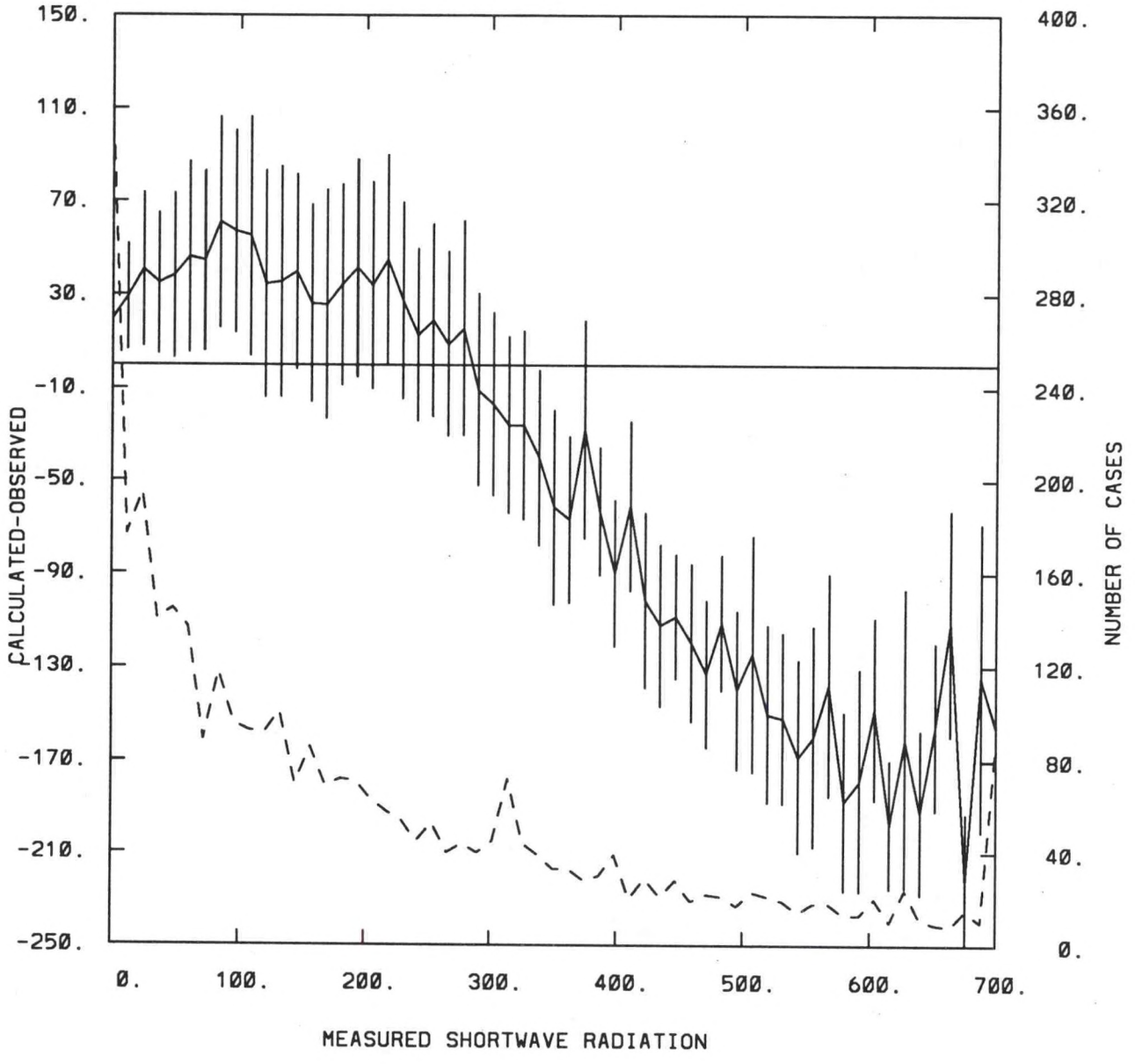
150.
110.
70.
30.
-10.
-50.
-90.
-130.
-170.
-210.
-250.
CALCULATED-OBSERVED
400.
360.
320.
280.
240.
200.
160.
120.
80.
40.
0.
NUMBER OF CASES
0.
100.
200.
300.
400.
500.
600.
700.
MEASURED SHORTWAVE RADIATION

Fig. 4

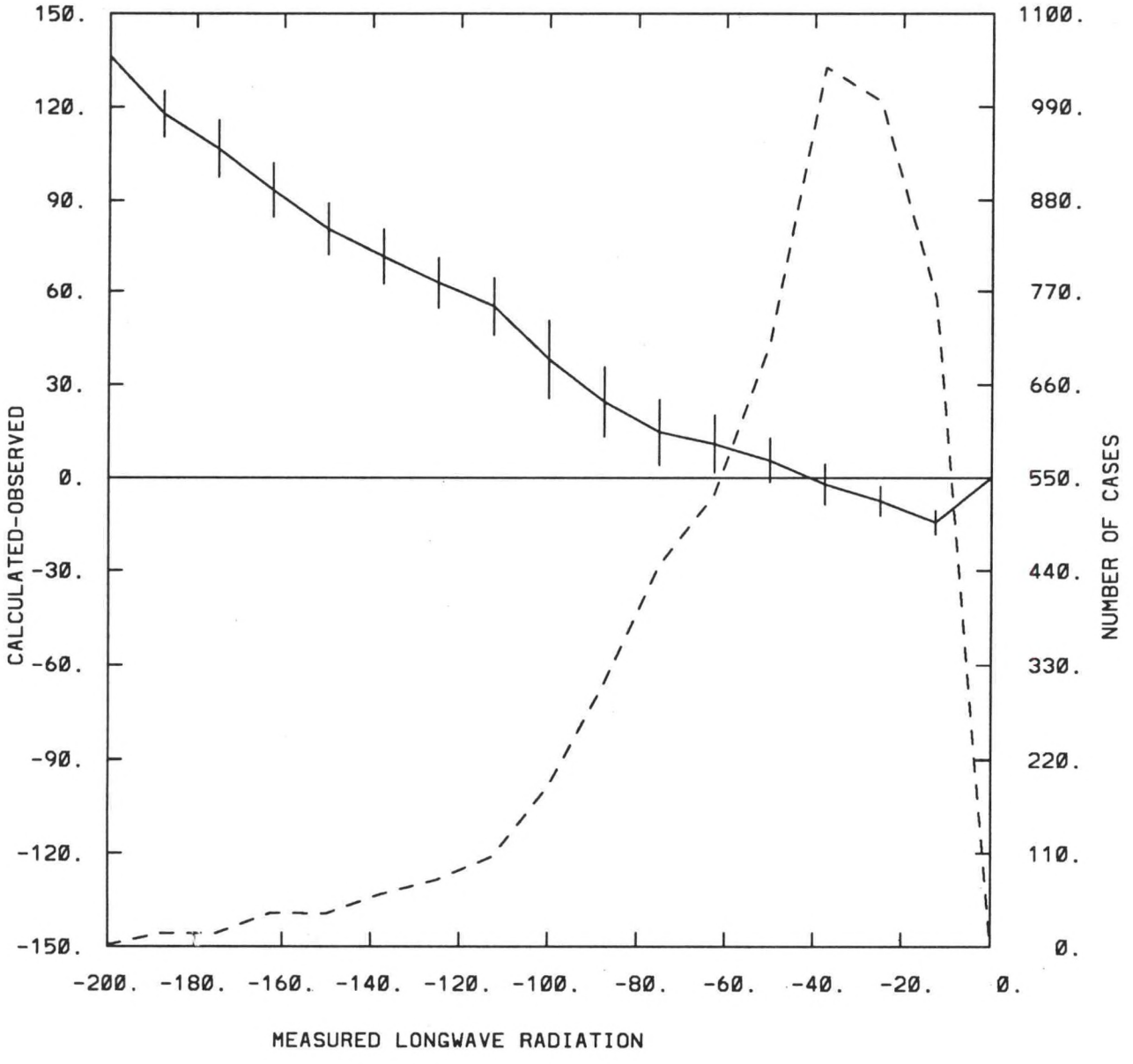
150.
120.
90.
60.
30.
0.
-30.
-60.
-90.
-120.
-150.
CALCULATED-OBSERVED
1100.
990.
880.
770.
660.
550.
440.
330.
220.
110.
0.
NUMBER OF CASES
-200. -180. -160. -140. -120. -100. -80. -60. -40. -20. 0.
MEASURED LONGWAVE RADIATION

Fig.5

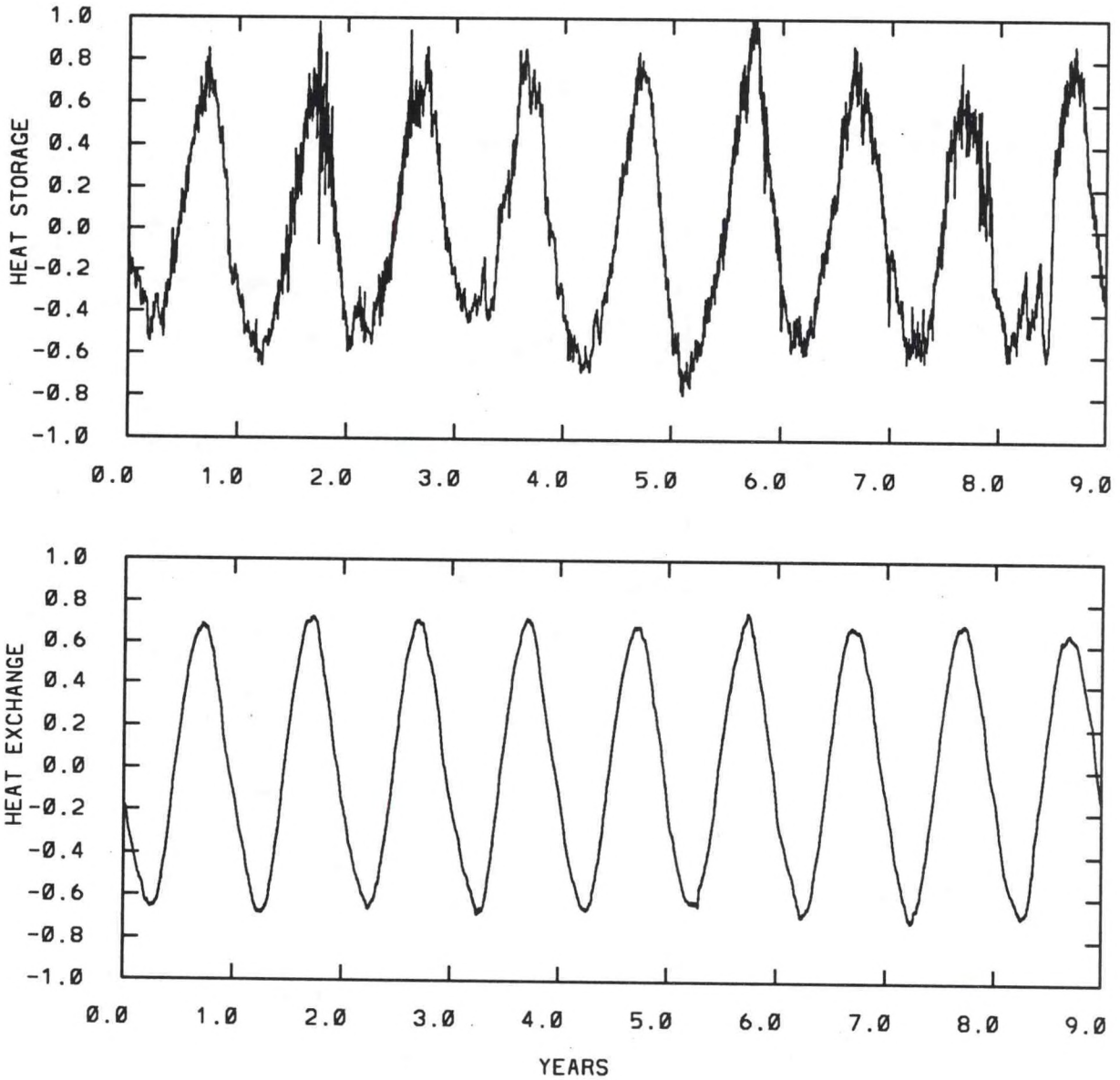
HEAT STORAGE
1.0
0.8
0.6
0.4
0.2
0.0
-0.2
-0.4
-0.6
-0.8
-1.0
0.0
1.0
2.0
3.0
4.0
5.0
6.0
7.0
8.0
9.0
HEAT EXCHANGE
1.0
0.8
0.6
0.4
0.2
0.0
-0.2
-0.4
-0.6
-0.8
-1.0
0.0
1.0
2.0
3.0
4.0
5.0
6.0
7.0
8.0
9.0
YEARS

Fig.6

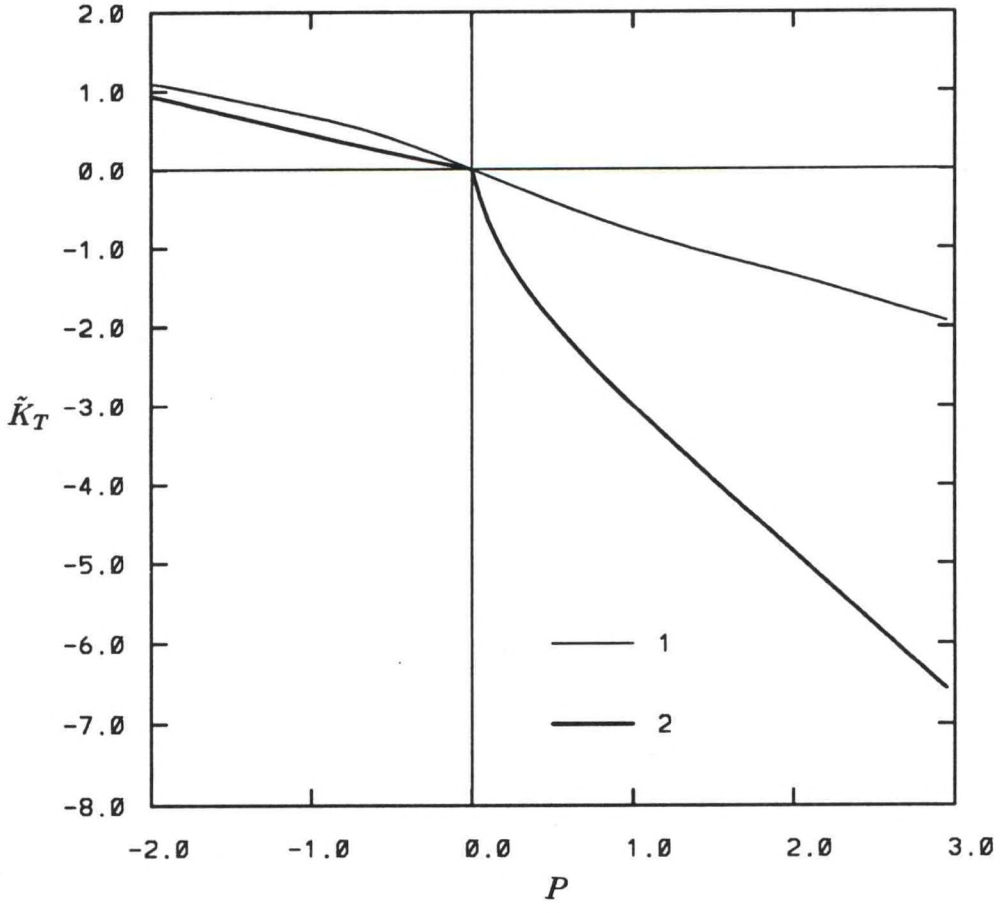

Fig.7

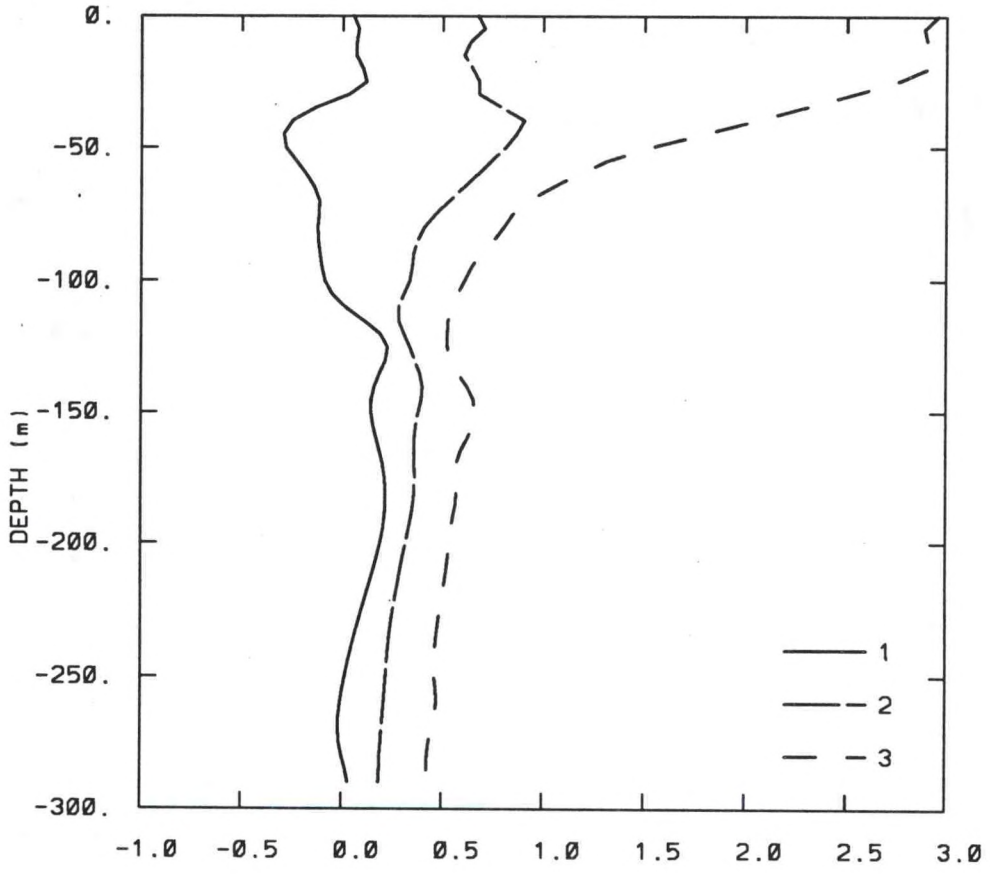

Fig. 8

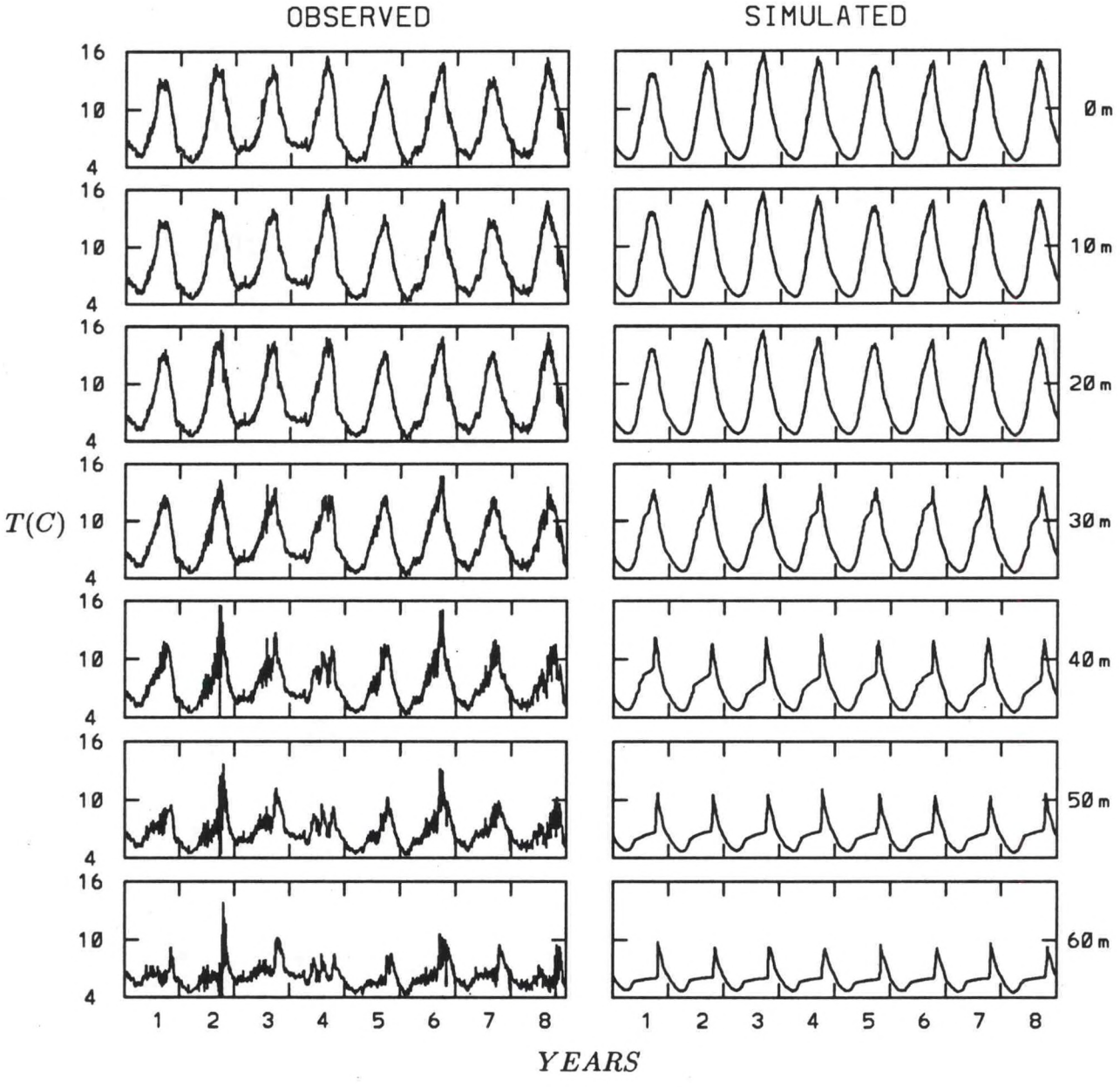
OBSERVED
SIMULATED
16
10
4
0m
10m
20m
30m
40m
50m
60m
T(C)
1 2 3 4 5 6 7 8
YEARS

Fig.9

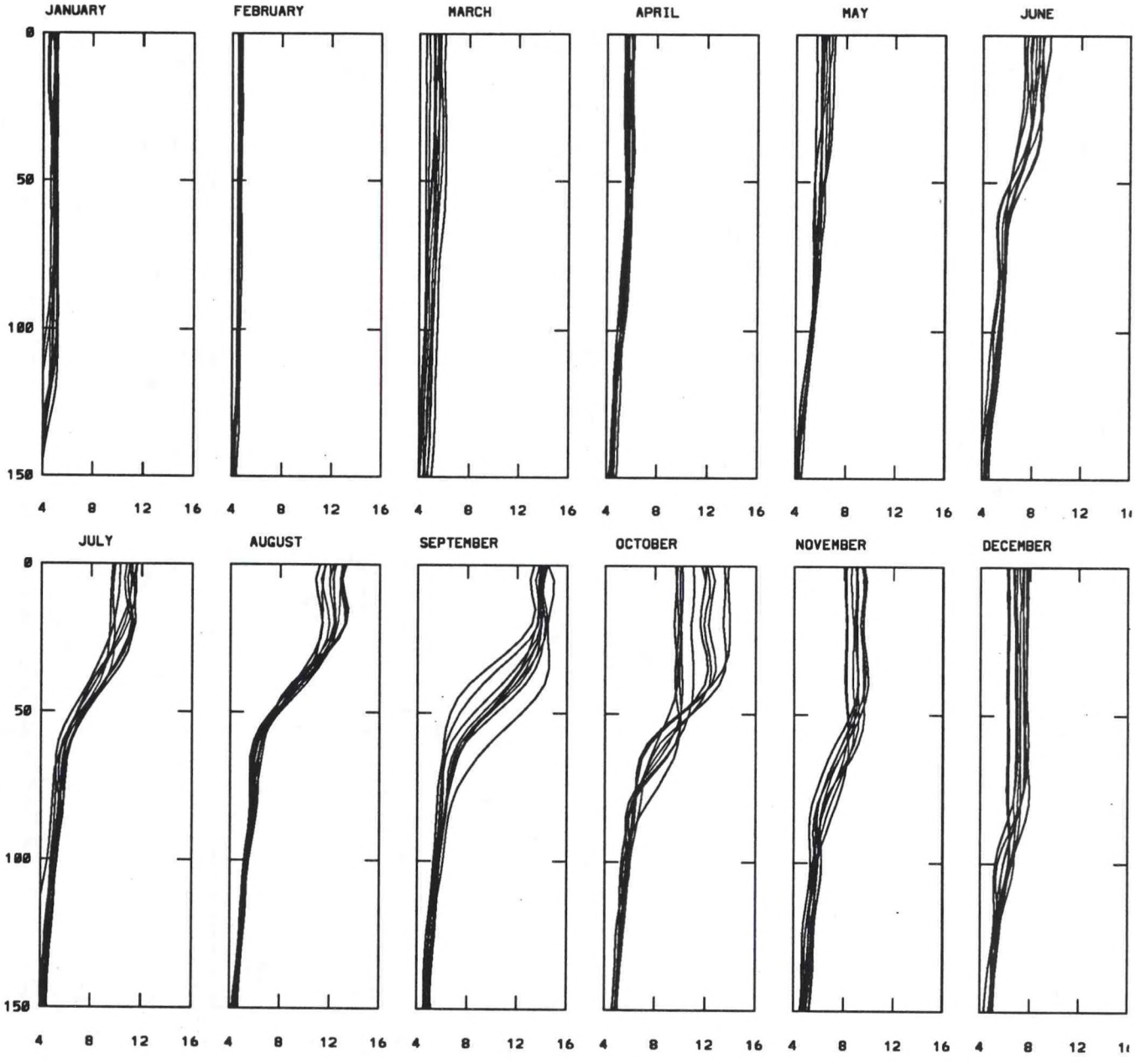
JANUARY
FEBRUARY
MARCH
APRIL
MAY
JUNE
JULY
AUGUST
SEPTEMBER
OCTOBER
NOVEMBER
DECEMBER
0
50
100
150
4
8
12
16

Fig. 10

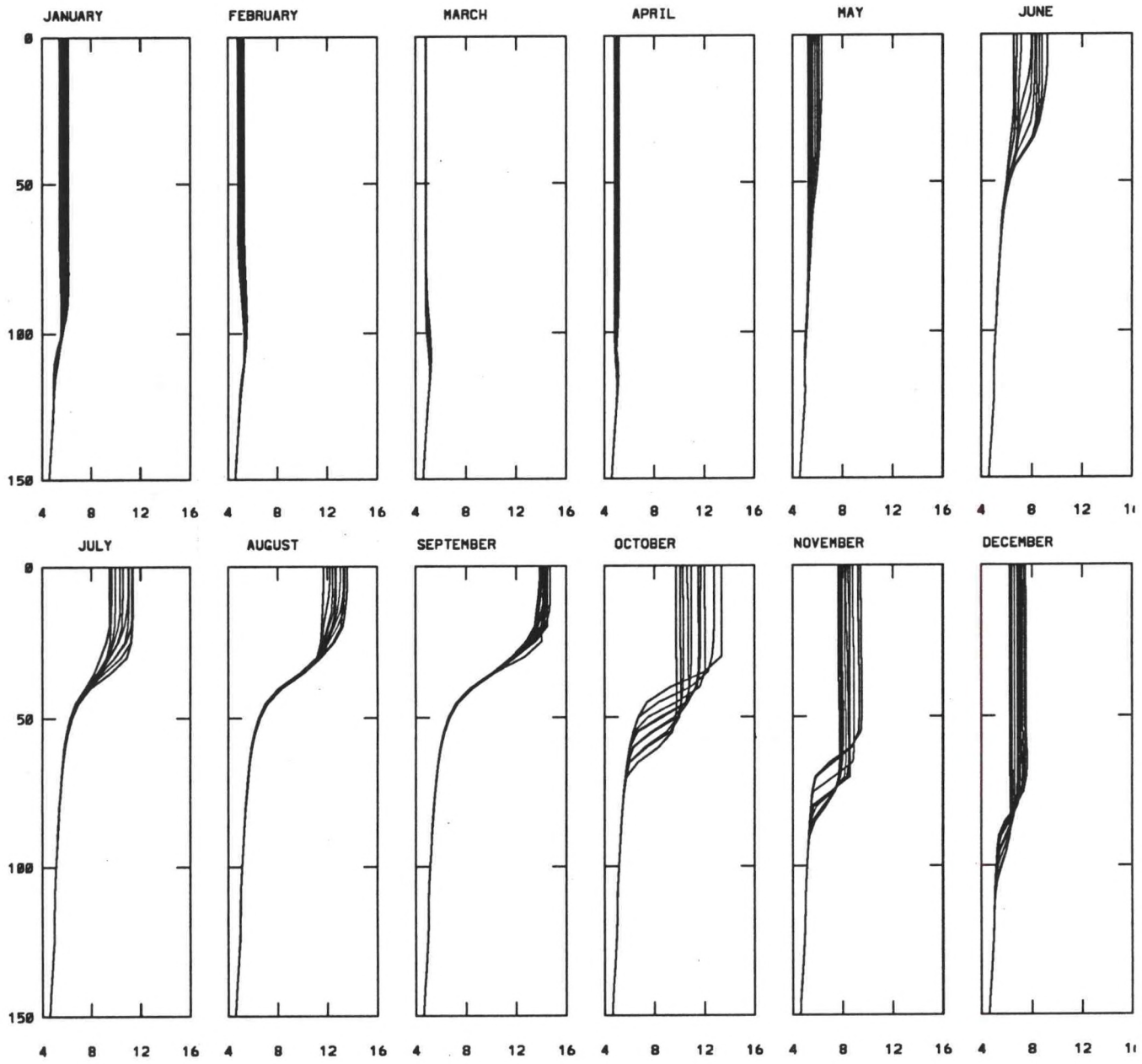
JANUARY
FEBRUARY
MARCH
APRIL
MAY
JUNE
JULY
AUGUST
SEPTEMBER
OCTOBER
NOVEMBER
DECEMBER
0
50
100
150
4
8
12
16

Fig. 11

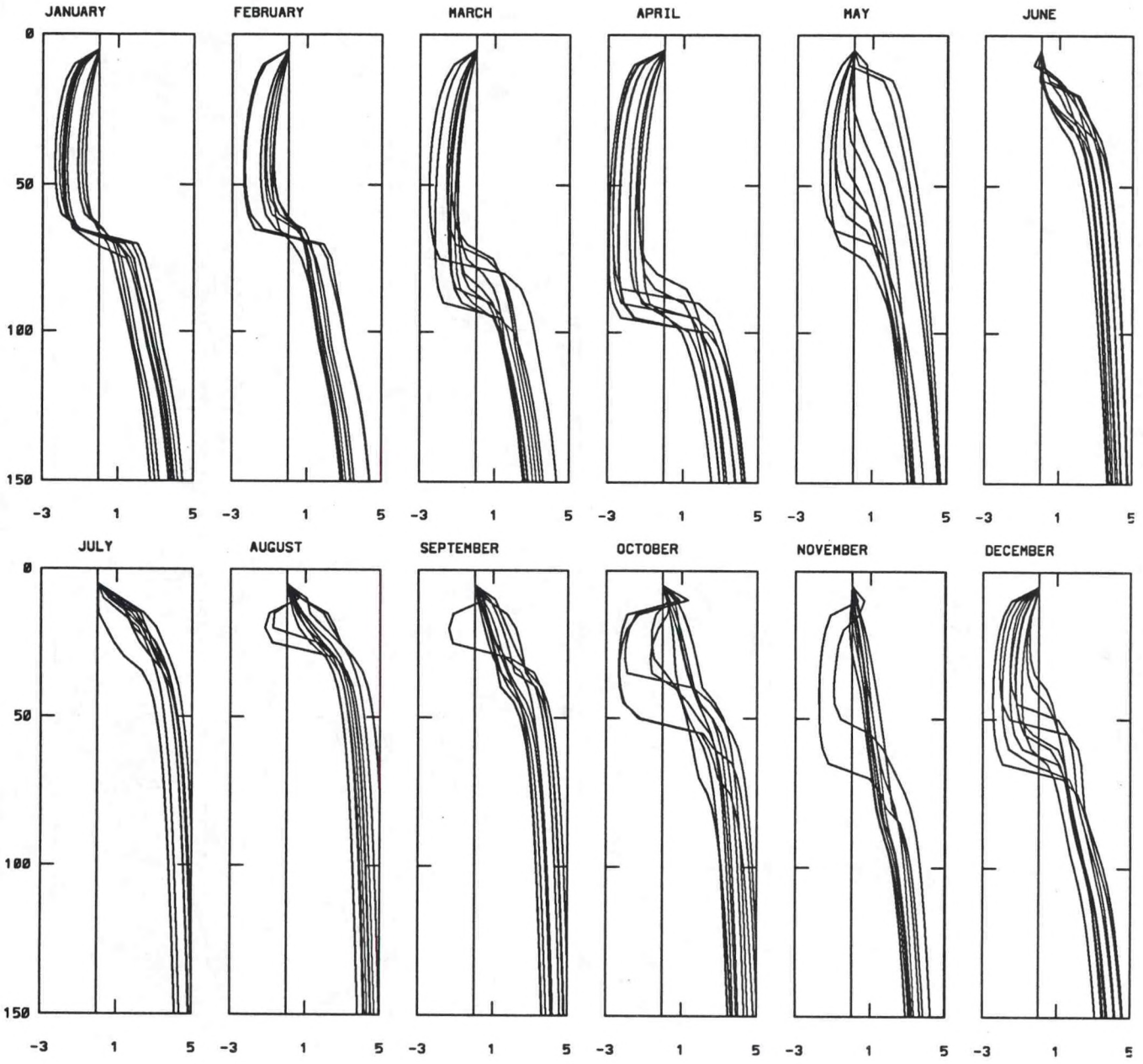
JANUARY
FEBRUARY
MARCH
APRIL
MAY
JUNE
JULY
AUGUST
SEPTEMBER
OCTOBER
NOVEMBER
DECEMBER
0
50
100
150
-3
1
5

Fig. 12

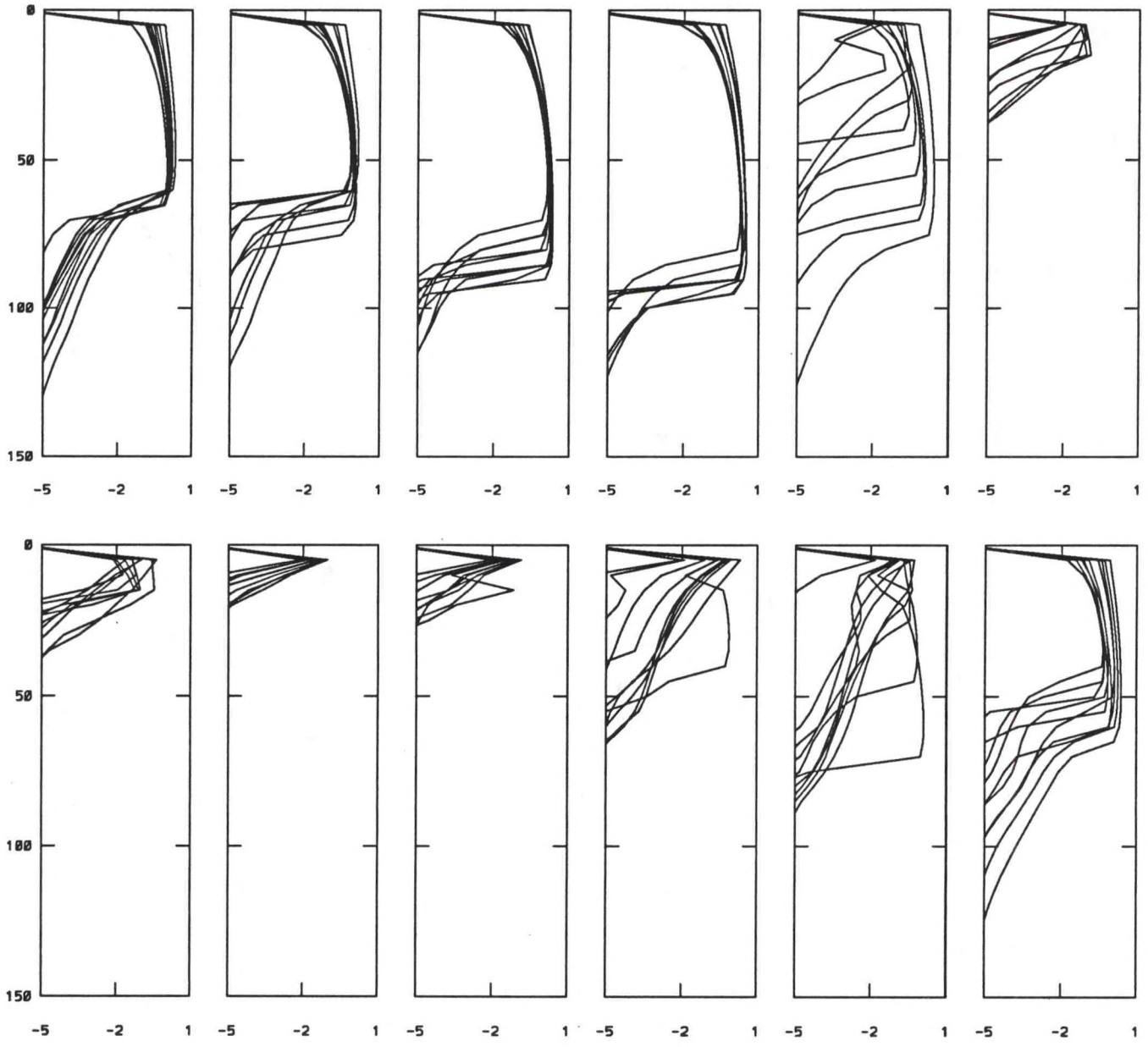

Fig. 13

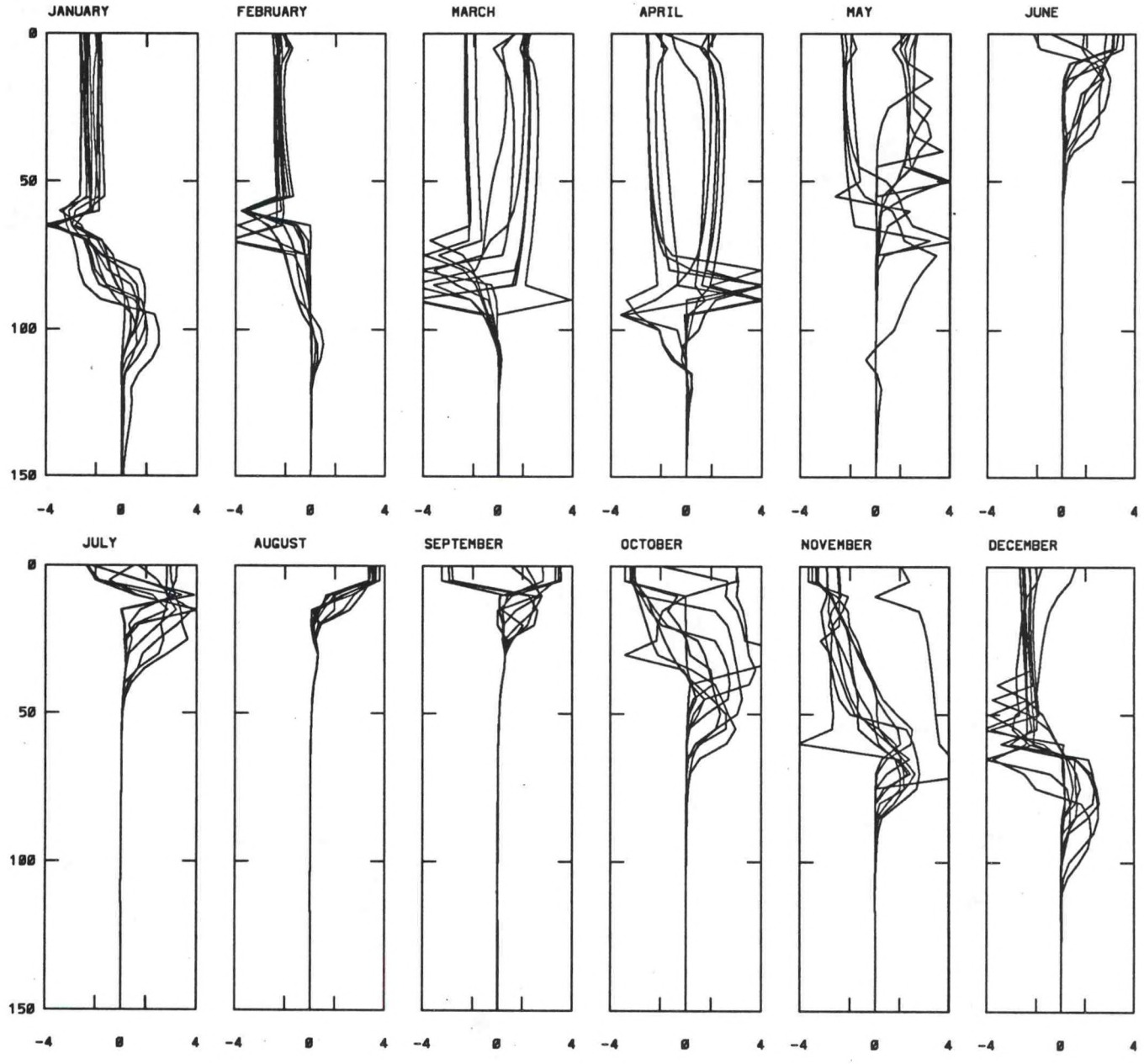
JANUARY
FEBRUARY
MARCH
APRIL
MAY
JUNE
JULY
AUGUST
SEPTEMBER
OCTOBER
NOVEMBER
DECEMBER
0
50
100
150
-4
0
4

Fig. 14

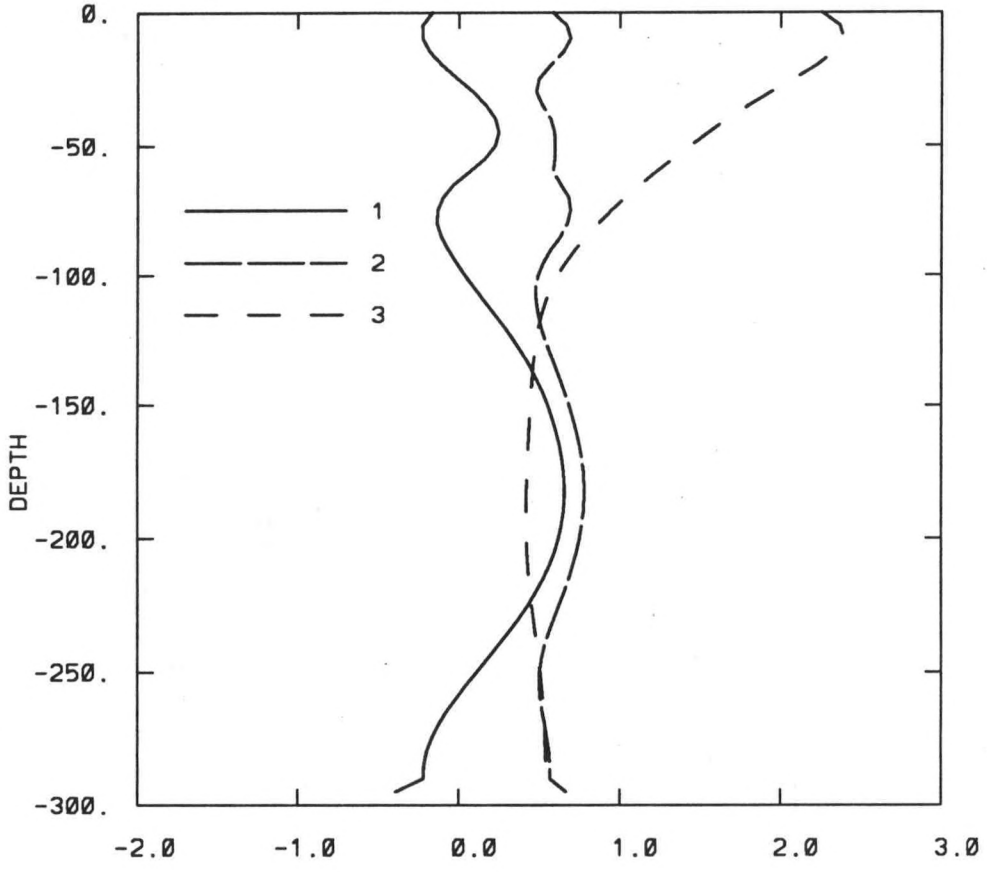

Fig. 15

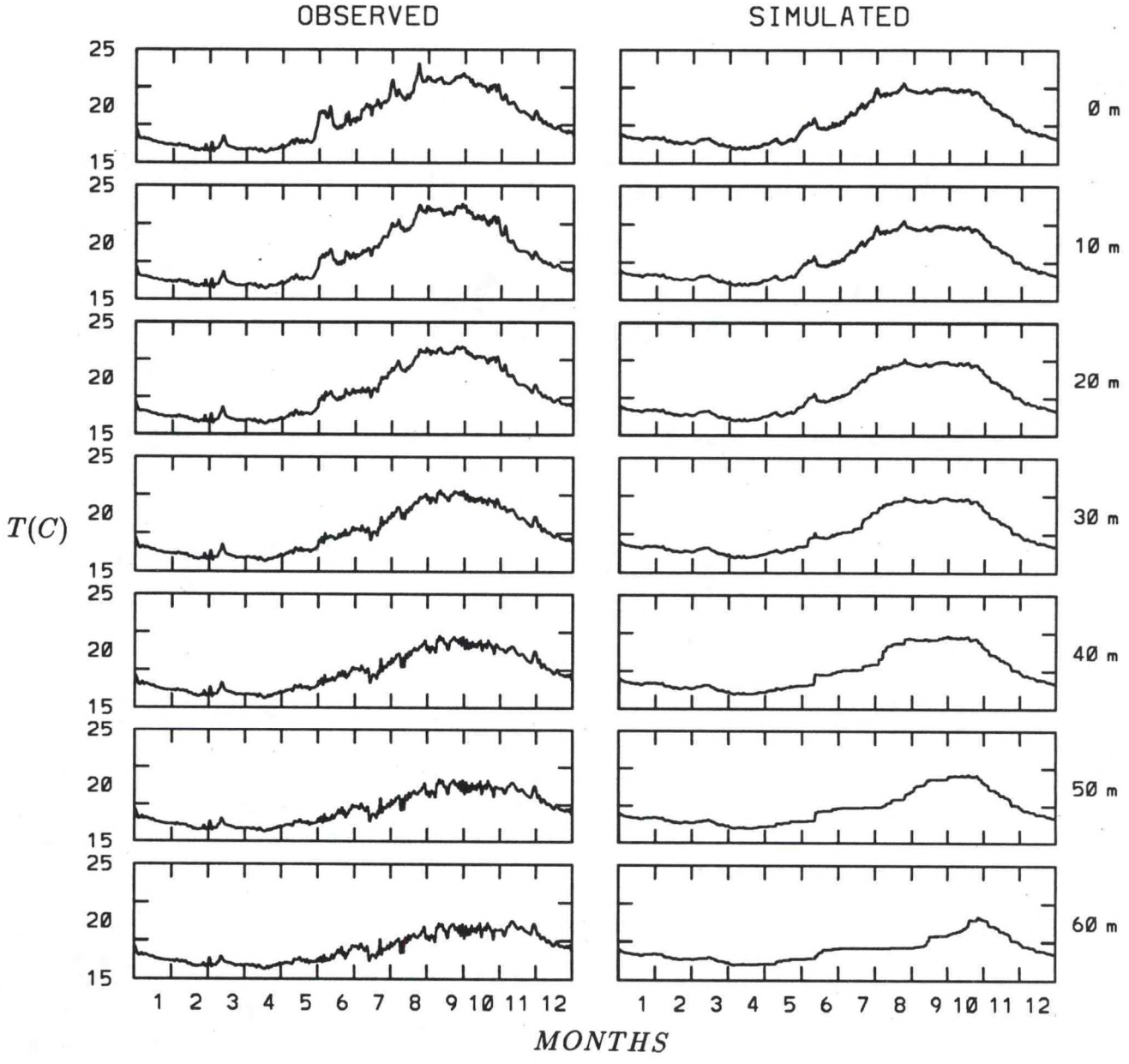
OBSERVED
SIMULATED
25
20
15
0 m
10 m
20 m
30 m
40 m
50 m
60 m
T(C)
1 2 3 4 5 6 7 8 9 10 11 12
MONTHS

Fig 16

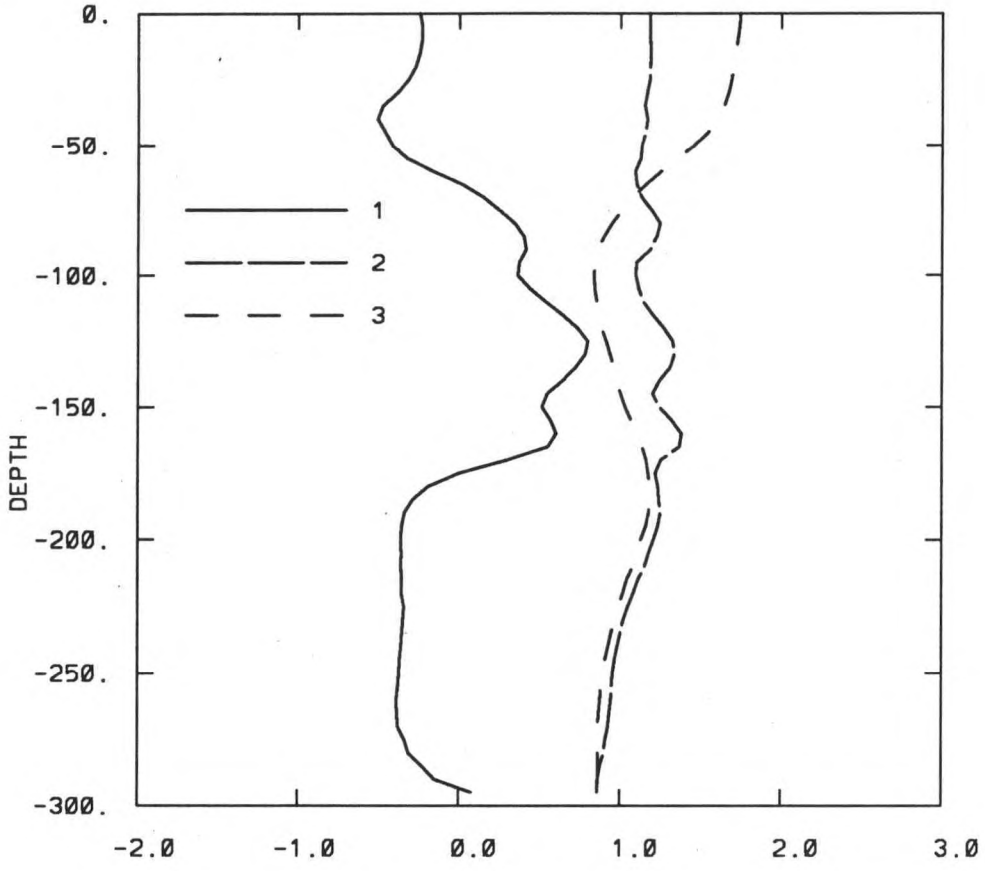

Fig 17

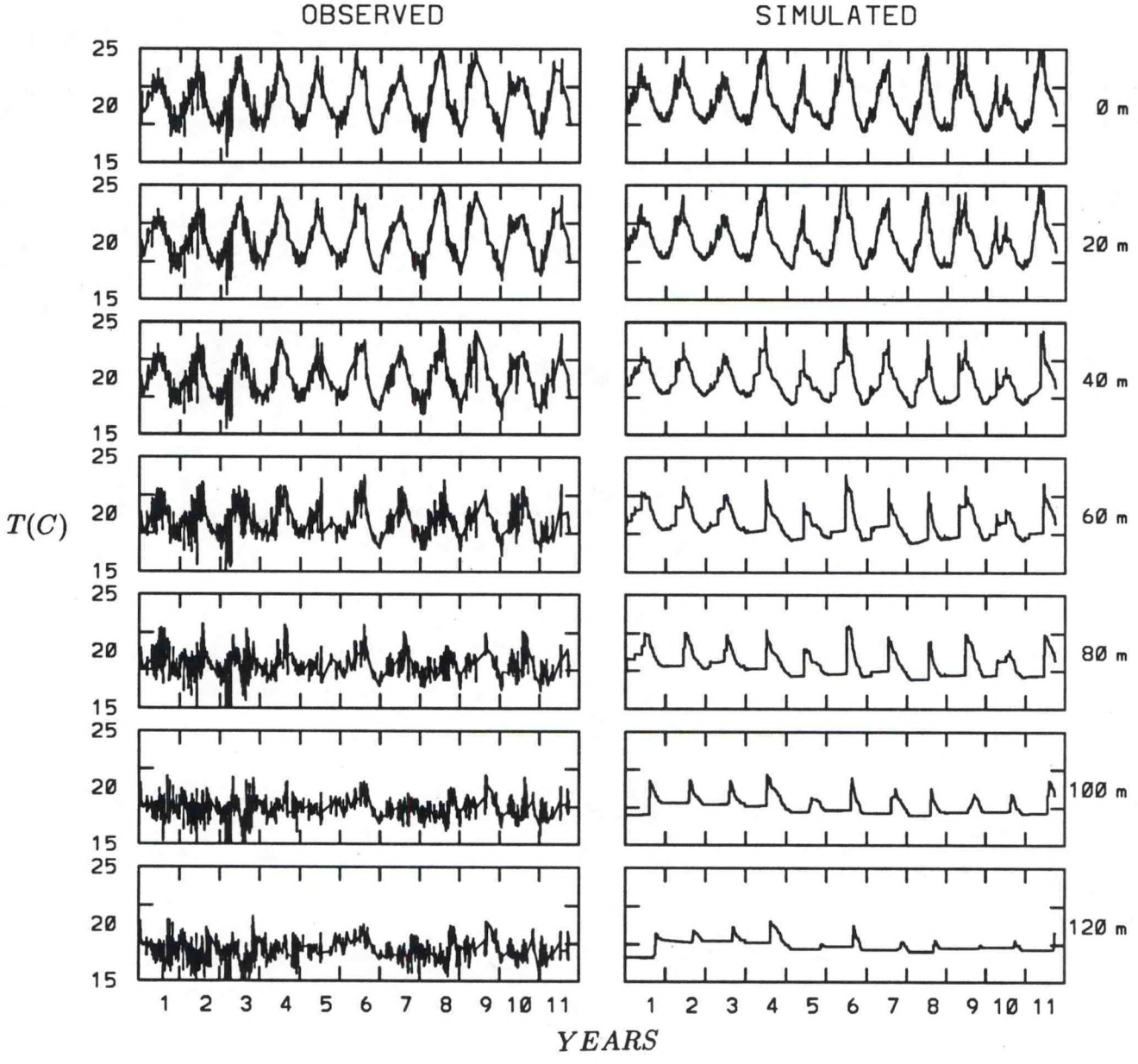
OBSERVED
SIMULATED
25
20
15
0 m
20 m
40 m
60 m
80 m
100 m
120 m
T(C)
1 2 3 4 5 6 7 8 9 10 11
YEARS

Fig. 18

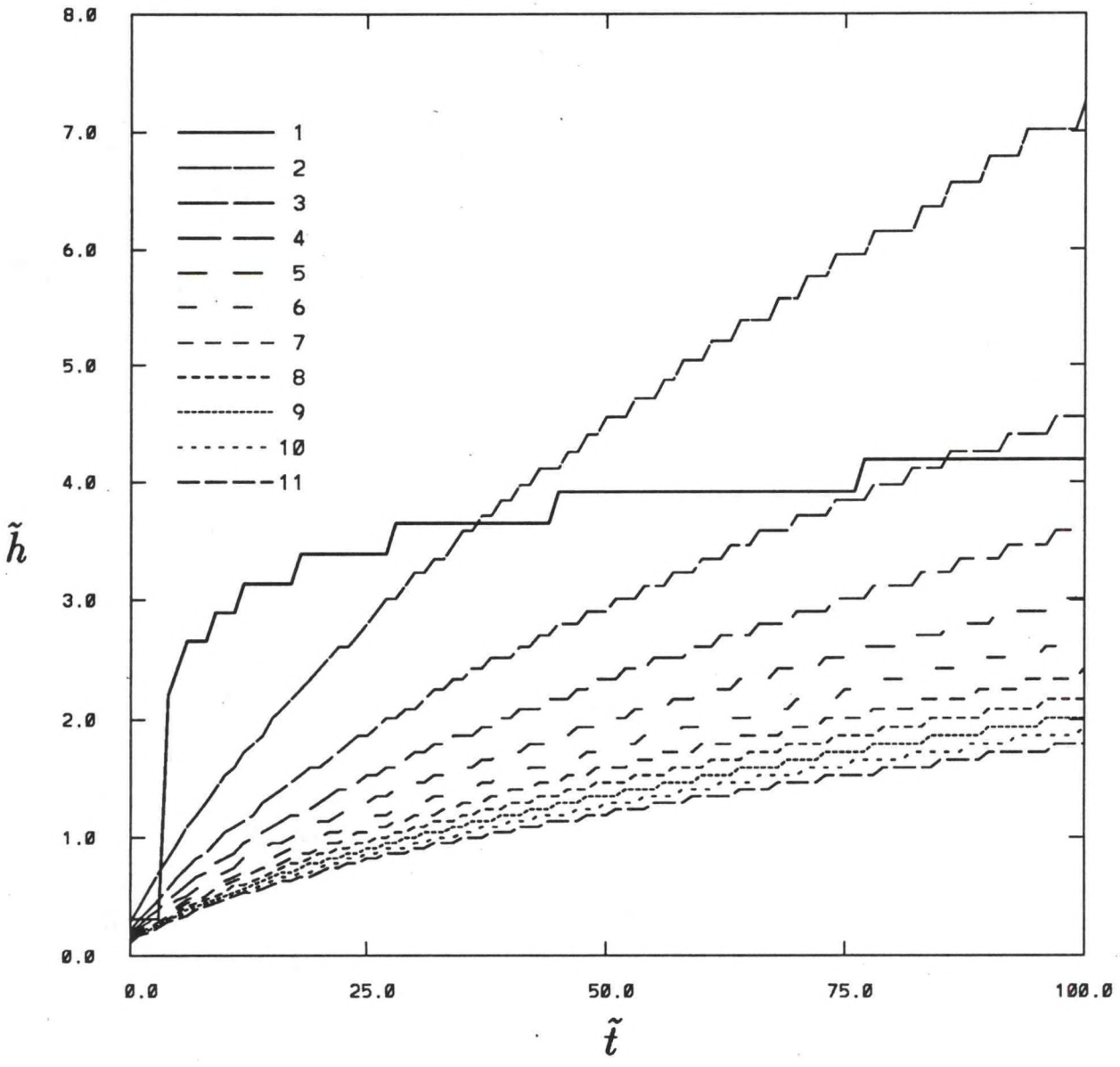
8.0
7.0
6.0
5.0
4.0
3.0
2.0
1.0
0.0
1
2
3
4
5
6
7
8
9
10
11
$\tilde{h}$
0.0
25.0
50.0
75.0
100.0
$\tilde{t}$

Fig. 19

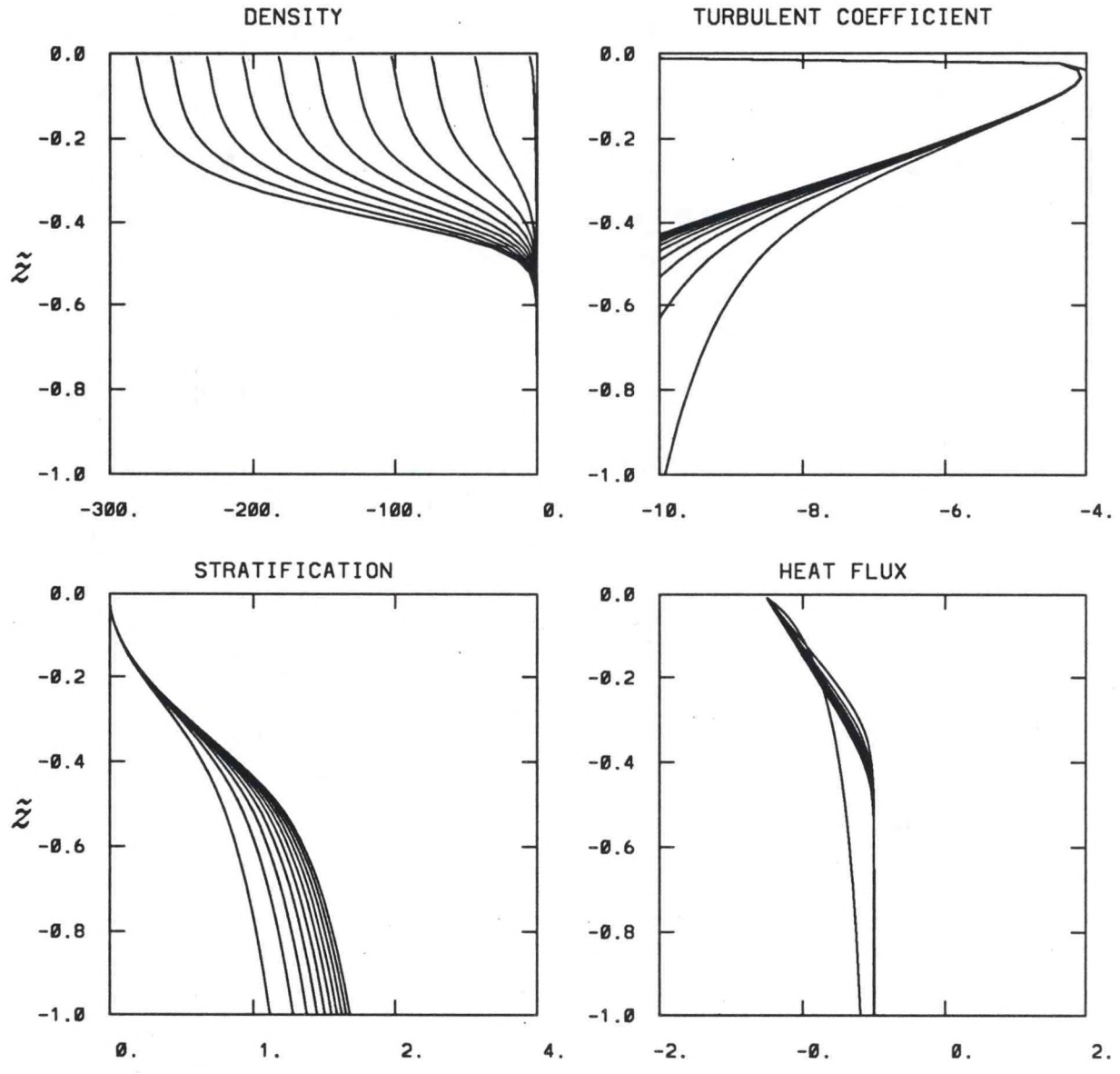
DENSITY
TURBULENT COEFFICIENT
STRATIFICATION
HEAT FLUX
0.0
-0.2
-0.4
-0.6
-0.8
-1.0
-300.
-200.
-100.
0.
-10.
-8.
-6.
-4.
1.
2.
4.
-2.
-0.
2.

Fig.20

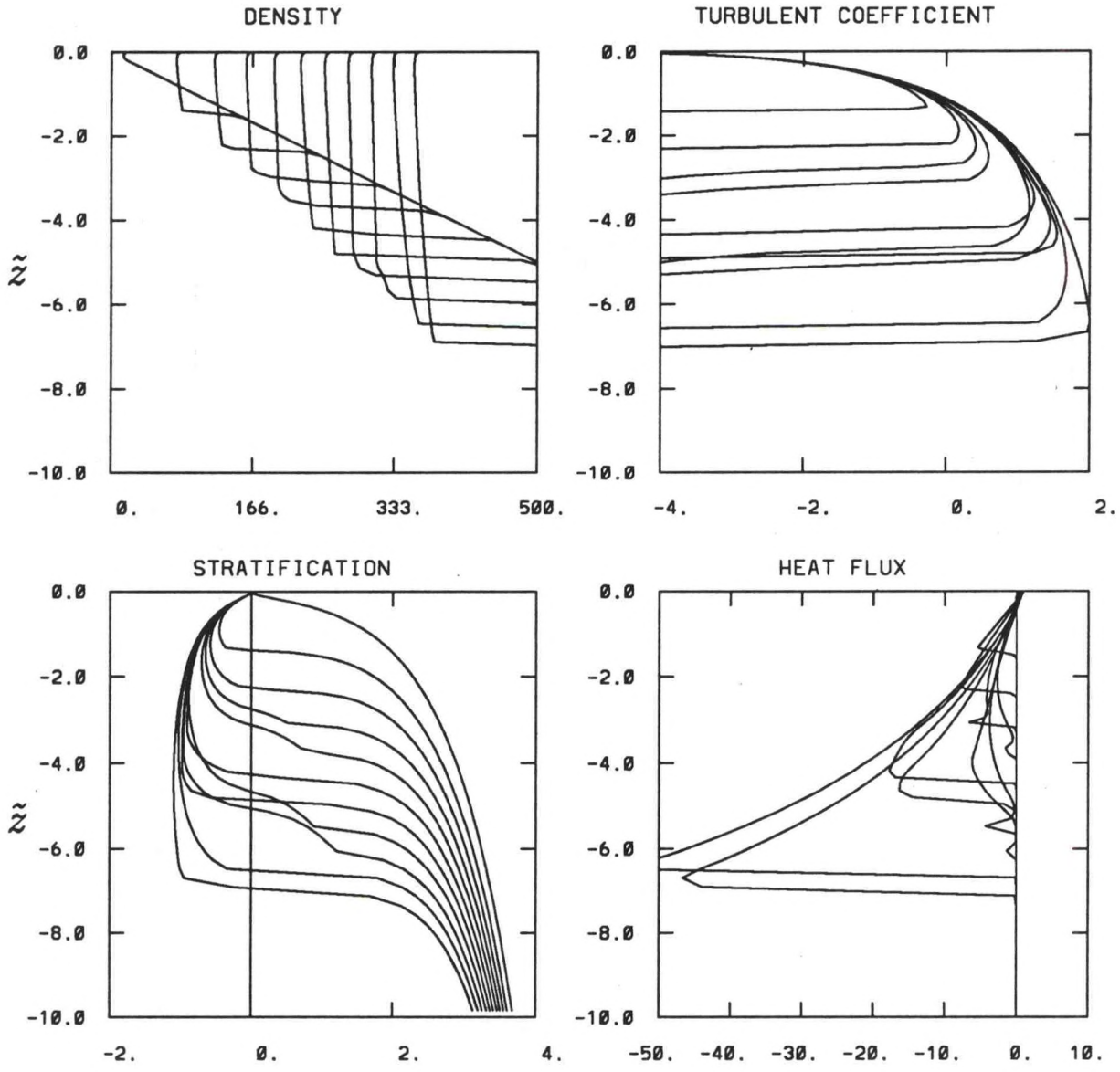
DENSITY
TURBULENT COEFFICIENT
STRATIFICATION
HEAT FLUX
0.0
-2.0
-4.0
-6.0
-8.0
-10.0
0.
166.
333.
500.
-4.
-2.
0.
2.
-2.
0.
2.
4.
-50.
-40.
-30.
-20.
-10.
0.
10.

Fig. 21

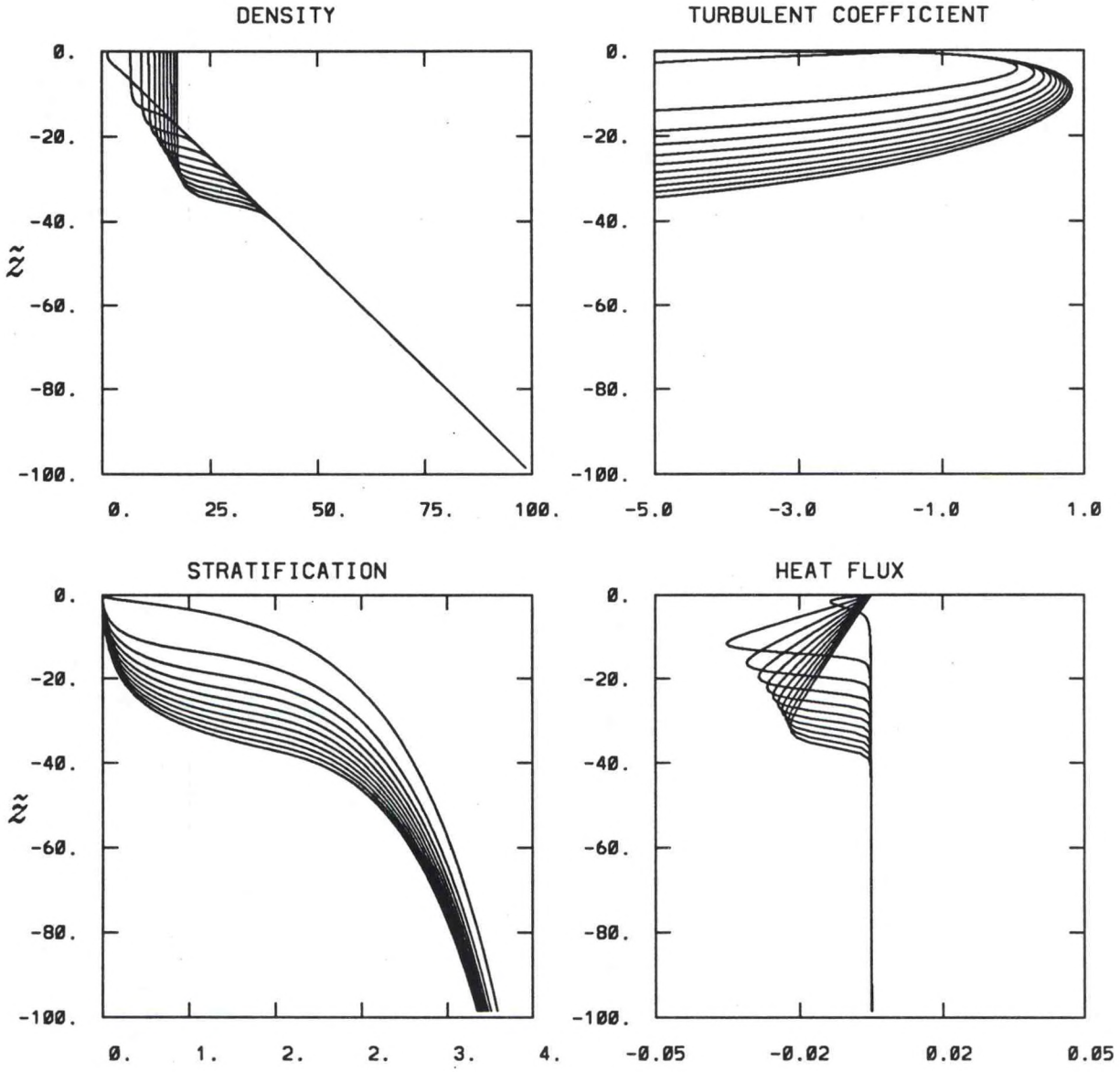
DENSITY
TURBULENT COEFFICIENT
STRATIFICATION
HEAT FLUX
0.
-20.
-40.
-60.
-80.
-100.
0.
25.
50.
75.
100.
-5.0
-3.0
-1.0
1.0
1.
2.
2.
3.
4.
-0.05
-0.02
0.02
0.05

Fig. 22

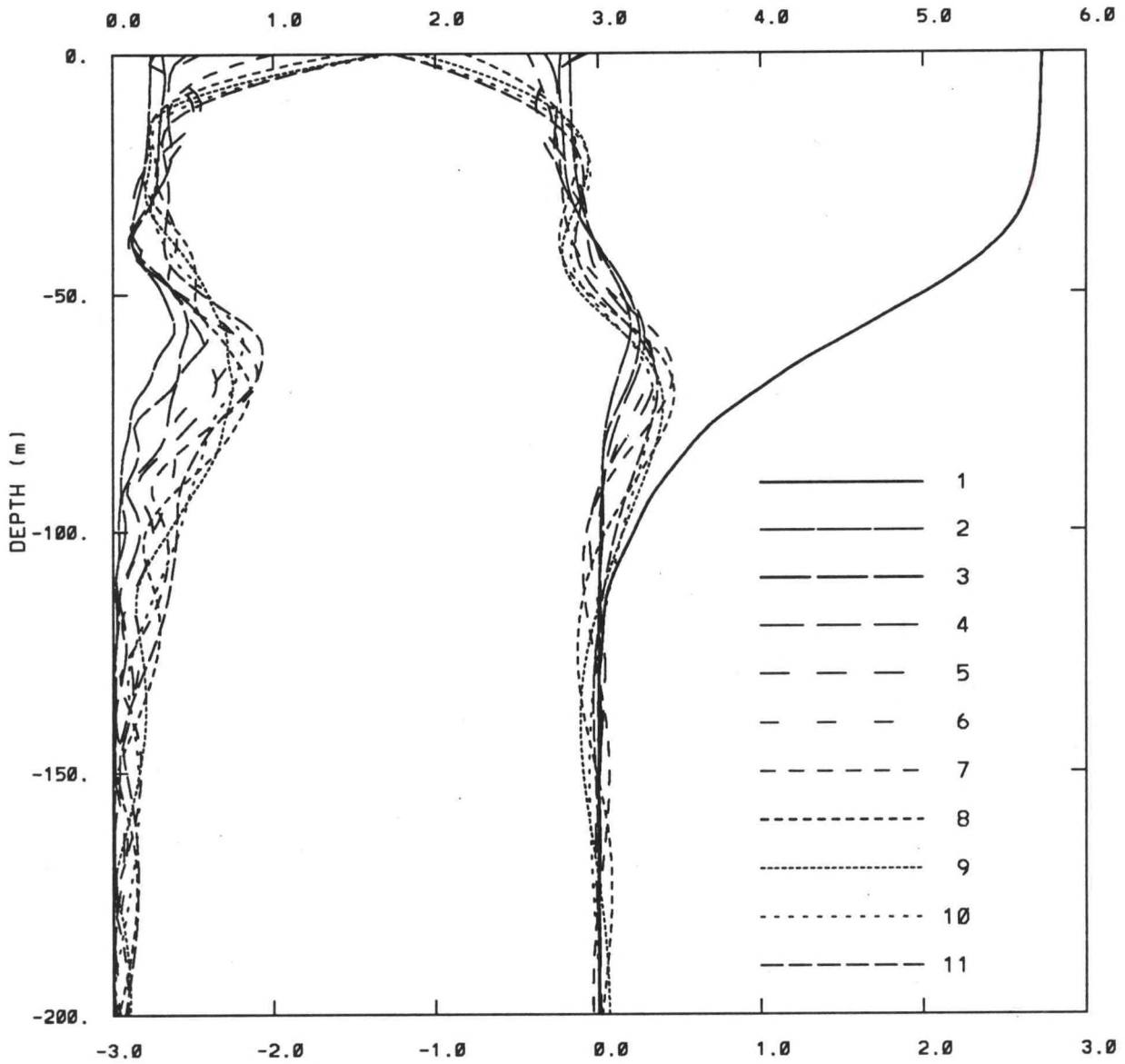
0.0
1.0
2.0
3.0
4.0
5.0
6.0
0.
-50.
-100.
-150.
-200.
DEPTH (m)
-3.0
-2.0
-1.0
0.0
1.0
2.0
3.0
1
2
3
4
5
6
7
8
9
10
11

Fig. 23

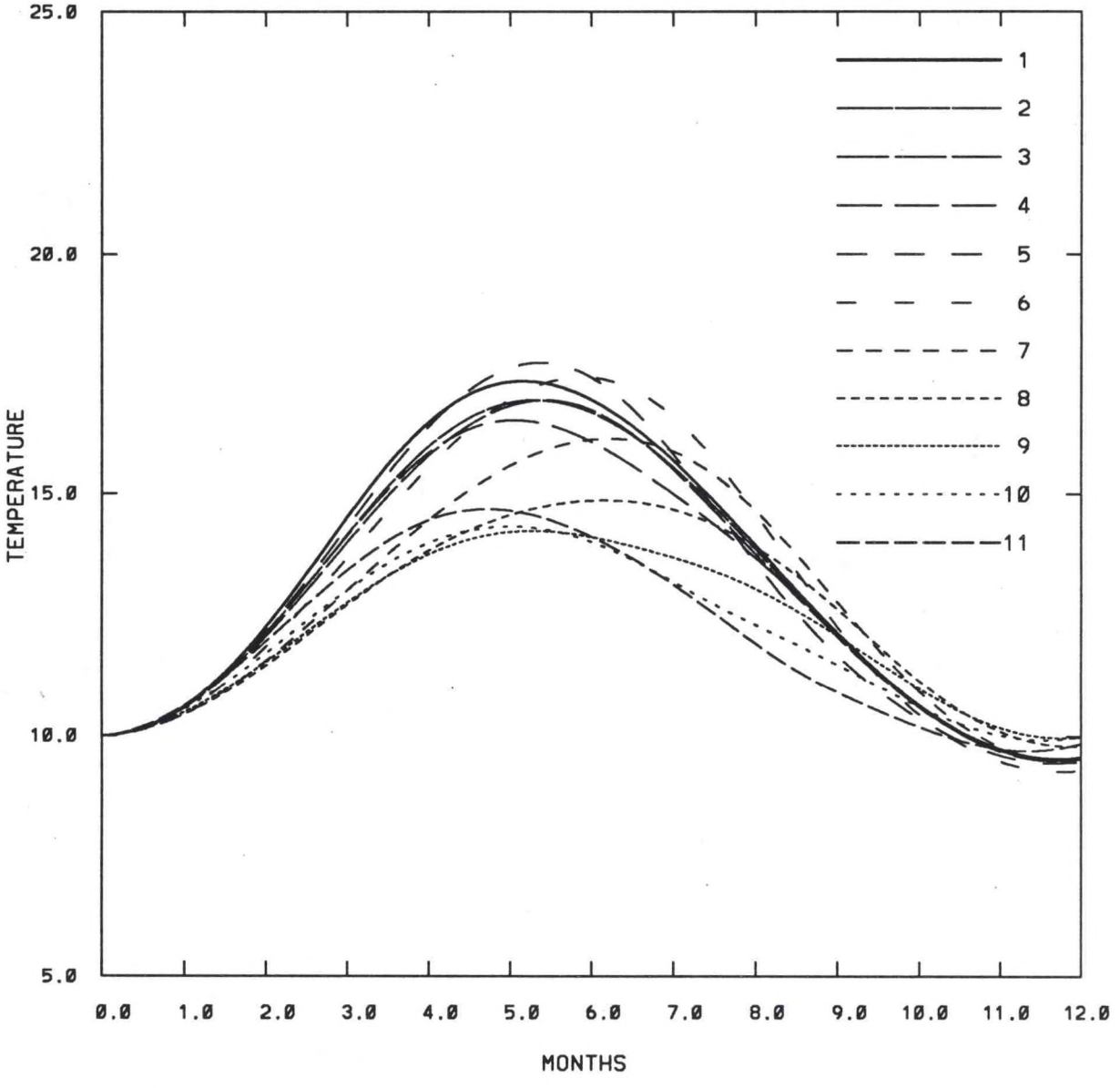
25.0
20.0
15.0
10.0
5.0
TEMPERATURE
0.0
1.0
2.0
3.0
4.0
5.0
6.0
7.0
8.0
9.0
10.0
11.0
12.0
MONTHS
1
2
3
4
5
6
7
8
9
10
11

Fig.24

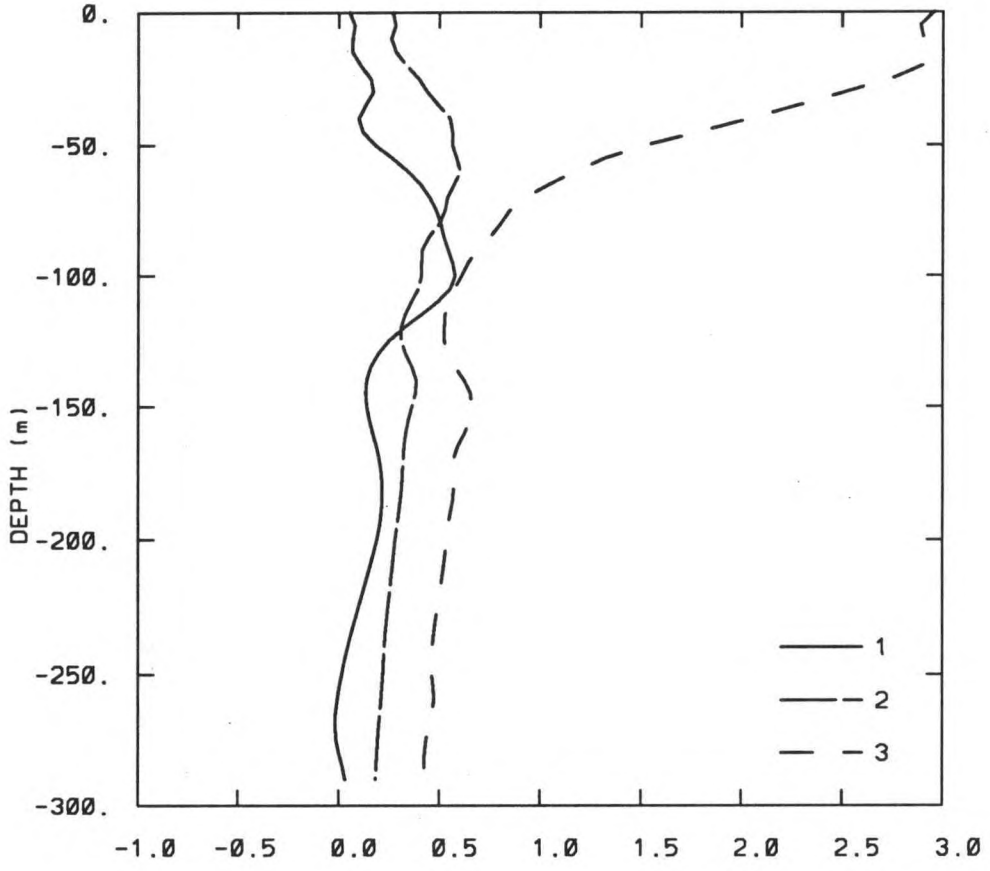

Fig. 25

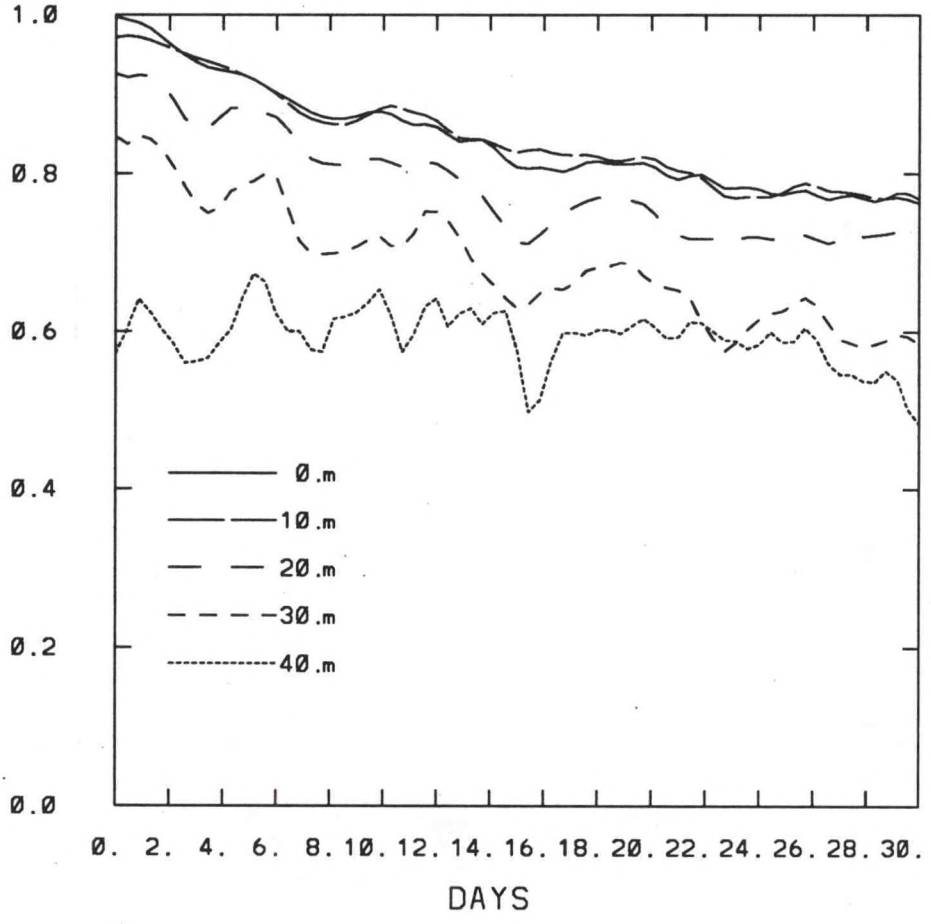
1.0
0.8
0.6
0.4
0.2
0.0
0. 2. 4. 6. 8. 10. 12. 14. 16. 18. 20. 22. 24. 26. 28. 30.
DAYS
0.m
10.m
20.m
30.m
40.m

OPC CONTRIBUTIONS (Cont.)

No. 21. Breaker, L. C., 1989: El Nino and Related Variability in Sea-Surface Temperature Along the Central California Coast. PACLIM Monograph of Climate Variability of the Eastern North Pacific and Western North America, Geophysical Monograph 55, AGU, 133-140.

No. 22. Yu, T. W., D. C. Esteva, and R. L. Teboulle, 1991: A Feasibility Study on Operational Use of Geosat Wind and Wave Data at the National Meteorological Center. Technical Note/NMC Office Note No. 380, 28pp.

No. 23. Burroughs, L. D., 1989: Open Ocean Fog and Visibility Forecasting Guidance System. Technical Note/NMC Office Note No. 348, 18pp.

No. 24. Gerald, V. M., 1987: Synoptic Surface Marine Data Monitoring. Technical Note/NMC Office Note No. 335, 10pp.

No. 25. Breaker, L. C., 1989: Estimating and Removing Sensor Induced Correlation form AVHRR Data. Journal of Geophysical Reseach, 95, 9701-9711.

No. 26. Chen, H. S., 1990: Infinite Elements for Water Wave Radiation and Scattering. International Journal for Numerical Methods in Fluids, 11, 555-569.

No. 27. Gemmill, W. H., T. W. Yu, and D. M. Feit, 1988: A Statistical Comparison of Methods for Determining Ocean Surface Winds. Journal of Weather and Forecasting, 3, 153-160.

No. 28. Rao. D. B., 1989: A Review of the Program of the Ocean Products Center. Weather and Forecasting, 4, 427-443.

No. 29. Chen, H. S., 1989: Infinite Elements for Combined Diffration and Refraction . Conference Preprint, Seventh International Conference on Finite Element Methods Flow Problems, Huntsville, Alabama, 6pp.

No. 30. Chao, Y. Y., 1989: An Operational Spectral Wave Forecasting Model for the Gulf of Mexico. Proceedings of 2nd International Workshop on Wave Forecasting and Hindcasting, 240-247.

No. 31. Esteva, D. C., 1989: Improving Global Wave Forecasting Incorporating Altimeter Data. Proceedings of 2nd International Workshop on Wave Hindcasting and Forecasting,Vancouver, B.C., April 25-28, 1989, 378-384.

No. 32. Richardson, W. S., J. M. Nault, and D. M. Feit, 1989: Computer-Worded Marine Forecasts. Preprint, 6th Symp. on Coastal Ocean Management Coastal Zone 89, 4075-4084.

No. 33. Chao, Y. Y., and T. L. Bertucci, 1989: A Columbia River Entrance Wave Forecasting Program Developed at the Ocean Products Center. Techical Note/NMC Office Note 361.

No. 34. Burroughs, L. D., 1989: Forecasting Open Ocean Fog and Visibility. Preprint, 11th Conference on Probability and Statisitcs, Monterey, Ca., 5pp.

No. 35. Rao, D. B., 1990: Local and Regional Scale Wave Models. Proceeding (CMM/WMO) Technical Conference on Waves, WMO, Marine Meteorological of Related Oceanographic Activities Report No. 12, 125-138.

No. 36. Burroughs, L.D., 1991: Forecast Guidance for Santa Ana conditions. Technical Procedures Bulletin No. 391, 11pp.

No. 37. Burroughs, L. D., 1989: Ocean Products Center Products Review Summary. Technical Note/NMC Office Note No. 359. 29pp.

No. 38. Feit, D. M., 1989: Compendium of Marine Meteorological and Oceanographic Products of the Ocean Products Center (revision 1). NOAA Technical Memo NWS/NMC 68.

No. 39. Esteva, D. C., and Y. Y. Chao, 1991: The NOAA Ocean Wave Model Hindcast for LEWEX. Directional Ocean Wave Spectra, Johns Hopkins University Press, 163-166.

No. 40. Sanchez, B. V., D. B. Rao, and S. D. Steenrod, 1987: Tidal Estimation in the Atlantic and Indian Oceans, 3° x 3° Solution. NASA Technical Memorandum 87812, 18pp.

No. 41. Crosby, D. S., L. C. Breaker, and W. H. Gemmill, 1990: A Defintion for Vector Correlation and its Application to Marine Surface Winds. Technical Note/NMC Office Note No. 365, 52pp.

No. 42. Feit, D. M., and W. S. Richardson, 1990: Expert System for Quality Control and Marine Forecasting Guidance. Preprint, 3rd Workshop Operational and Metoerological. CMOS, 6pp.

No. 43. Gerald, V. M., 1990: OPC Unified Marine Database Verification System. Technical Note/NMC Office Note No. 368, 14pp.

No. 44. Wohl, G. M., 1990: Sea Ice Edge Forecast Verification System. National Weather Association Digest, (submitted)

No. 45. Feit, D. M., and J. A. Alpert, 1990: An Operational Marine Fog Prediction Model. NMC Office Note No. 371, 18pp.

No. 46. Yu, T. W., and R. L. Teboulle, 1991: Recent Assimilation and Forecast Experiments at the National Meteorological Center Using SEASAT-A Scatterometer Winds. Technical Note/NMC Office Note No. 383, 45pp.

No. 47. Chao, Y. Y., 1990: On the Specification of Wind Speed Near the Sea Surface. Marine Forecaster Training Manual.

No. 48. Breaker, L. C., L. D. Burroughs, T. B. Stanley, and W. B. Campbell, 1992: Estimating Surface Currents in the Slope Water Region Between 37 and 41°N Using Satellite Feature Tracking. Technical Note, 47pp.

No. 49. Chao, Y. Y., 1990: The Gulf of Mexico Spectral Wave Forecast Model and Products. Technical Procedures Bulletin No. 381, 3pp.

No. 50. Chen, H. S., 1990: Wave Calculation Using WAM Model and NMC Wind. Preprint, 8th ASCE Engineering Mechanical Conference, 1, 368-372.

No. 51. Chao, Y. Y., 1990: On the Transformation of Wave Spectra by Current and Bathymetry. Preprint, 8th ASCE Engineering Mechnical Conference, 1, 333-337.

No. 52. WAS NOT PUBLISHED

No. 53. Rao, D. B., 1991: Dynamical and Statistical Prediction of Marine Guidance Products. Proceedings, IEEE Conference Oceans 91, 3, 1177-1180.

No. 54. Gemmill, W. H., 1991: High-Resolution Regional Ocean Surface Wind Fields. Proceedings, AMS 9th Conference on Numerical Weather Prediction, Denver, CO, Oct. 14-18, 1991, 190-191.

No. 55. Yu, T. W., and D. Deaven, 1991: Use of SSM/I Wind Speed Data in NMC's GDAS. Proceedings, AMS 9th Conference on Numerical Weather Prediction, Denver, CO, Oct. 14-18, 1991, 416-417.

No. 56. Burroughs, L. D., and J. A. Alpert, 1993: Numerical Fog and Visiability Guidance in Coastal Regions. Technical Procedures Bulletin. No. 398, 6pp.

No. 57. Chen, H. S., 1992: Taylor-Gelerkin Method for Wind Wave Propagation. ASCE 9th Conf. Eng. Mech. (in press)

No. 58. Breaker, L. C., and W. H. Gemmill, and D. S. Crosby, 1992: A Technique for Vector Correlation and its Application to Marine Surface Winds. AMS 12th Conference on Probability and Statistics in the Atmospheric Sciences, Toronto, Ontario, Canada, June 22-26, 1992.

No. 59. Yan, X.-H., and L. C. Breaker, 1993: Surface Circulation Estimation Using Image Processing and Computer Vision Methods Applied to Sequential Satellite Imagery. Photogrammetric Engineering and Remote Sensing, 59, 407-413.

No. 60. Wohl, G., 1992: Operational Demonstration of ERS-1 SAR Imagery at the Joint Ice Center. Proceeding of the MTS 92 - Global Ocean Partnership, Washington, DC, Oct. 19-21, 1992.

No. 61. Waters, M. P., Caruso, W. H. Gemmill, W. S. Richardson, and W. G. Pichel, 1992: An Interactive Information and Processing System for the Real-Time Quality Control of Marine Meteorological Oceanographic Data. Pre-print 9th International Conference on Interactive Information and Processing System for Meteorology, Oceanography and Hydrology, Anaheim, CA, Jan. 17-22, 1993.

No. 62. Breaker, L. C., and V. Krasnopolsky, 1994: The Problem of AVHRR Image Navigation Revisited. Int. Journal of Remote Sensing, 15, 979-1008.

No. 63. Crosby, D. S., L. C. Breaker, and W. H. Gemmill, 1993: A Proposed Definition for Vector Correlation in Geophysics: Theory and Application. Journal of Atmospheric and Ocean Technology, 10, 355-367.

No. 64. Grumbine, R., 1993: The Thermodynamic Predictability of Sea Ice. Journal of Glaciology, 40, 277-282, 1994.

No. 65. Chen, H. S., 1993: Global Wave Prediction Using the WAM Model and NMC Winds. 1993 International Conference on Hydro Science and Engineering, Washington, DC, June 7 - 11, 1993. (submitted)

No. 66. WAS NOT PUBLISHED

No. 67. Breaker, L. C., and A. Bratkovich, 1993: Coastal-Ocean Processes and their Influence on the Oil Spilled off San Francisco by the M/V Puerto Rican. Marine Environmental Research, 36, 153-184.

No. 68. Breaker, L. C., L. D. Burroughs, J. F. Culp, N. L. Gunasso, R. Teboulle, and C. R. Wong, 1993: Surface and Near-Surface Marine Observations During Hurricane Andrew. Technical Note/NMC Office Note #398, 41pp.

No. 69. Burroughs, L. D., and R. Nichols, 1993: The National Marine Verification Program - Concepts and Data Management, Technical Note/NMC Office Note #393, 21pp.

No. 70. Gemmill, W. H., and R. Teboulle, 1993: The Operational Use of SSM/I Wind Speed Data over Oceans. Pre-print 13th Conference on Weather Analyses and Forecasting, AMS Vienna, VA., August 2-6, 1993, 237-238.

No. 71. Yu, T.-W., J. C. Derber, and R. N. Hoffman, 1993: Use of ERS-1 Scatterometer Backscattered Measurements in Atmospheric Analyses. Pre-print 13th Conference on Weather Analyses and Forecasting, AMS, Vienna, VA., August 2-6, 1993, 294-297.

No. 72. Chalikov, D. and Y. Liberman, 1993: Director Modeling of Nonlinear Waves Dynamics. J. Physical, (To be submitted).

No. 73. Woiceshyn, P., T. W. Yu, W. H. Gemmill, 1993: Use of ERS-1 Scatterometer Data to Derive Ocean Surface Winds at NMC. Pre-print 13th Conference on Weather Analyses and Forecasting, AMS, Vienna, VA, August 2-6, 1993, 239-240.

No. 74. Grumbine, R. W., 1993: Sea Ice Prediction Physics. Technical Note/NMC Office Note #396, 44pp.

No. 75. Chalikov, D., 1993: The Parameterization of the Wave Boundary Layer. Journal of Physical Oceanography, Vol. 25, No. 6, Par 1, 1333-1349.

No. 76. Tolman, H. L., 1993: Modeling Bottom Friction in Wind-Wave Models. Ocean Wave Measurement and Analysis, O.T. Magoon and J.M. Hemsley Eds., ASCE, 769-783.

No. 77. Breaker, L., and W. Broenkow, 1994: The Circulation of Monterey Bay and Related Processes. Oceanography and Marine Biology: An Annual Review, 32, 1-64.

No. 78. Chalikov, D., D. Esteva, M. Iredell and P. Long, 1993: Dynamic Coupling between the NMC Global Atmosphere and Spectral Wave Models. Technical Note/NMC Office Note #395, 62pp.

No. 79. Burroughs, L. D., 1993: National Marine Verification Program - Verification Statistics - Verification Statistics, Technical Note/NMC Office Note #400, 49 pp.

No. 80. Shashy, A. R., H. G. McRandal, J. Kinnard, and W. S. Richardson, 1993: Marine Forecast Guidance from an Interactive Processing System. 74th AMS Annual Meeting, January 23 - 28, 1994.

No. 81. Chao, Y. Y., 1993: The Time Dependent Ray Method for Calculation of Wave Transformation on Water of Varying Depth and Current. Wave 93 ASCE.

No. 82. Tolman, H. L., 1994: Wind-Waves and Moveable-Bed Bottom Friction. Journal of Physical Oceanography, 24, 994-1009.

No. 83. Grumbine, R. W., 1993: Notes and Correspondence A Sea Ice Albedo Experiment with the NMC Meduim Range Forecast Model. Weather and Forecasting, (submitted).

No. 84. Chao, Y. Y., 1993: The Gulf of Alaska Regional Wave Model. Technical Procedure Bulletin, No. 427, 10 pp.

No. 85. Chao, Y. Y., 1993: Implementation and Evaluation of the Gulf of Alaska Regional Wave Model. Technical Note, 35 pp.

No. 86. WAS NOT PUBLISHED.

No. 87. Burroughs, L., 1994: Portfolio of Operational and Development Marine Meteorological and Oceanographic Products. Technical Note/NCEP Office Note No. 412, 52 pp. [PB96-158548]

No. 88. Tolman, H. L., and D. Chalikov, 1994: Development of a third-generation ocena wave model at NOAA-NMC. Proc. Waves Physical and Numberial Modelling, M. Isaacson and M.C. Quick Eds., Vancover, 724-733.

No. 89. Peters, C., W. H. Gemmill, V. M. Gerald, and P. Woiceshyn, 1994: Evaluation of Empirical Transfer Functions for ERS-1 Scatterometer Data at NMC. 7th Conference on Satellite Meteorology and Oceanography, June 6-10, 1994, Monterey, CA., pg. 550-552.

No. 90. Breaker, L. C., and C. R. N. Rao, 1996: The Effects of Aerosols from the Mt. Pinatubo and Mt. Hudson Volcanio Eruption on Satellite-Derived Sea Surface Temperatures. Journal of Geophysical Research. (To be submitted).

No. 91. Yu, T-W., P. Woiceshyn, W. Gemmill, and C. Peters, 1994: Analysis & Forecast Experiments at NMC Using ERS-1 Scatterometer Wind Measurements. 7th Conference on Satellite Meteorology and Oceanography, June 6-10, 1994, Monterey, CA., pg. 600-601.

No. 92. Chen, H. S., 1994: Ocean Surface Waves. Technical Procedures Bulletin, No. 426, 17 pp.

No. 93. Breaker, L. C., V. Krasnopolsky, D. B. Rao, and X.-H. Yan, 1994: The Feasibility of Estimating Ocean Surface Currents on an Operational Basis using Satellite Feature Tracking Methods. Bulletin of the American Meteorolgical Society, 75, 2085-2095.

No. 94. Krasnopolsky V., L. C. Breaker, and W. H. Gemmill, 1994: Development of Single "All-Weather" Neural Network Algorithms for Estimating Ocean Surface Winds from the Special Sensor Microwave Imager. Technical Note.

No. 95. Breaker, L. C., D. S. Crosby and W. H. Gemmill, 1994: The application of a New Definition for Vector Correlation to Problems in Oceanography and Meteorology. Journal of Applied Meteolorology, 33, 1354-1365.

No. 96. Peters, C. A., V. M. Gerald, P. M. Woiceshyn, and W. H. Gemmill, 1994: Operational Processing of ERS-1 Scatterometer winds: A Documentation. Technical Note.

No. 97. Gemmill, W. H., P. M. Woiceshyn, C. A. Peters, and V. M. Gerald, 1994: A Preliminary Evaluation Scatterometer Wind Transfer Functions for ERS-1 Data. Technical Note.

No. 98. Chen, H. S., 1994: Evaluation of a Global Ocean Wave Model at NMC. International Conference on Hydro-Science and Engineering. Beijing, China, March 22 - 26, 1995.

No. 99. Aikman, F. and D. B. Rao, 1994: NOAA Perspective on a Coastal Forecast System.

No. 100. Rao, D. B. and C. Peters, 1994: Two-Dimensional Co-Oscillations in a Rectangular Bay: Possible Application to Water-Level Problems. Marine Geodesy, 18, 317-332.

No. 101. Breaker, L. C., L. D. Burroughs, Y. Y. Chao, J. F. Culp, N. L. Gunasso, R. Teboulle, and C. R. Wong, 1994: Surface and Near-Surface Marine Observations During Hurricane Andrew. Weather and Forecasting, 9, 542-556.

No. 102. Tolman, H. L., 1995: Subgrid Modeling of Moveable-bed Bottom Friction in Wind Wave Models. Coastal Engineering, (in press).

No. 103. Breaker, L. C., D. B. Gilhousen, H. L. Tolman and L. D. Burroughs, 1995: Initial Results from Long-Term Measurements of Atmospheric Humidity and Related Parameters the Marine Boundary Layer at Two Locations in the Gulf of Mexico. (To be submitted to Global Atmosphere and Ocean Systems).

No. 104. Burroughs, L. D., and J. P. Dallavalle, 1995: Great Lakes Wind and Wave Guidance. Technical Procedures Bulletin No., (In preparation).

No. 105. Burroughs, L. D., and J. P. Dallavalle, 1995: Great Lakes Storm Surge Guidance. Technical Procedures Bulletin No., (In preparation).

No. 106. Shaffer, W. A., J. P. Dallavalle, and L. D. Burroughs, 1995: East Coast Extratropical Storm Surge and Beach Erosion Guidance. Technical Procedures Bulletin No., (In preparation)

No. 107. WAS NOT PUBLISHED.

No. 108. WAS NOT PUBLISHED.

No. 109. WAS NOT PUBLISHED.

No. 110. Gemmill, W. H, and C. A. Peters, 1995: The Use of Satellite Dervired Wind Data in High-Resolution Regional Ocean Surface Wind Fields. Conference on Coastal Oceanic and Atmospheric Prediction, Jan 28 - Feb 2, 1996, Atlanta, GA (accepted at preprint press).

OPC CHANGES TO OMB

No. 111. Krasnopolsky, V. M, W. H. Gemmill, and L. C. Breaker, 1995: Improved SSM/I Wind Speed Retrievals at Higher Wind Speeds. Journal of Geophysical Research, (in press).

No. 112. Chalikov, D., L. D. Breaker, and L. Lobocki, 1995: A Simple Model of Mixing in the Upper Ocean. Journal of Physical Ocean, (in press).

No. 113. Tolman, H. L., 1995: On the Selection of Propagation Schemes for a Spectral Wind-Wave Model. NCEP Office Note No. 411.

No. 114. Grumbine, R. W., 1995: Virtual Floe Ice Drift Forecast Model Intercomparison. NCEP Office Note. (To be submitted).

No. 115. Grumbine, R. W., 1995: Sea Ice Forecast Model Intercomparison: Selecting a Base Model for NCEP Sea Ice Modelling. Technical Note.

No. 116. Yu, T. W. and J. C. Derber, 1995: Assimilation Experiments with ERS-1 Winds: Part I - Use of Backscatter Measurements in the NMC Spectral Statistical Analysis System. Technical Note.

No. 117. Yu, T. W., 1995: Assimilation Experiments with ERS1 Winds: Part II - Use of Vector Winds in NCEP Spectral Statistical Analysis System. Technical Note.

No. 118. Grumbine, R. W., 1995: Sea Ice Drift Guidance. Technical Procedures Bulletin. (submitted)

No. 119. Tolman, H. L., 1996: Statistical Model Validation Techniques Applied to Marine Wind Speed Analysis. Technical Note.

No. 120. Grumbine, R. W., 1996: Automated Passive Microwave Sea Ice Concentration Analysis at NCEP. Technical Note.

No. 121. Grumbine, R. W., 1996: Sea Ice Prediction Environment: Documentation. Technical Note.

No. 122. Tolman, H. L and D. Chalikov, 1996: On the Source Terms in a Third-Generation Wind Wave Model. Journal of Physical Oceanography. (To be submitted).

No. 123. Gemmill, W. H., V. Krasnopolsky, L. C. Breaker, and C. Peters, 1996: Developments to Improve Satellite Derived Ocean Surface Winds for use in Marine Analyses. Pre-print Numerical Weather Prediction Conference, Norfolk, VA, Aug. 19-23, 1996.

No. 124. Breaker, L. C., D. B. Gilhousen, H. L. Tolman and L. D. Burroughs, 1996: Initial Results from Long-Term Measurements of Atmospheric Humidity and Related Parameters in the Marine Boundary Layer at Two Locations in the Gulf of Mexico. NCEP Office Note No. 414.

No. 125. Yu, T. W., M. D. Iredell, and Y. Zhu, 1996: The Impact of ERS-1 Winds on NCEP Operational Numerical Weather Analyses and Forecast. Pre-print Numerical Weather Predicition Conference, Norfolk, VA, August 19-23, 1996.

No. 126. Burroughs, L. D., 1996: Marine Meteorological and Oceanographic Guidance Products from the National Centers for Environmental Prediction. Mariners Weather Log. (To be submitted).

No. 127. Lobocki, L., 1996: Coastal Ocean Forecasting System (COFS) System Description and User Guides. Technical Note.

No. 128. WAS NOT PUBLISHED

No. 129. Chailkov, D., 1996: A Global Ocean Model. Technical Note.

No. 130. Yu, T.W., 1996: Applications of SSM/I Wind Speed Data to NCEP Regional Analyses. Technical Note.

No. 131. Chailkov, D. and D. Sheinin, 1996: Direct Modeling of 1-D Nonlinear Potential Waves. Advances in Fluid Mechanics Series: Nonlinear Ocean Waves (submitted).

No. 132. Krasnopolsky, V. M., W. H. Gemmill, L. C. Breaker, and V. Y. Raizer, 1996: SSM/I Wind Speed Retrieval Algorithm with Improved Performance at Higher Wind Speed. Remote Sensing of Environment (submitted).

No. 133. Yu, T. W., 1996: The Effect of Drifting Buoy Data on NCEP Numerical Weather Forecast. Technical Note.

No. 134. Krasnopolsky, V. M., 1996: A Neural Network Forward Model for Direct Assimilation of SSM/I Brightness Temperatures into Atmospheric Models. CAS/JSC Working Group on Numerical Experimentation (in press).

No. 135. Krasnopolsky, V. M., W. H. Gemmill, and L. C. Breaker, 1996: A New Neural Network Transfer for SSM/I Retrievals. CAS/JSC Working Group on Numerical Experimentation (in press).

No. 136. Krasnopolsky, V. M., 1996: NN Solutions for Forward & Inverse Problems in Satellite Remote Sensing. 1997 International Conference on Neural Networks (ICNN 97). (submitted).

No. 137. Krasnopolsky, V. M., 1996: A New Neural Network Transfer Function for SSM/I Based on an Expanded Neural Network Architecture. Technical Note.

No. 138. Chailkov, D. C., L. C. Breaker, and L. Lobocki, 1996: Parameterization of Mixing in Upper Ocean. Technical Note.

No. 139. Chailkov, D. C., and D. Sheinin, 1996: Numerical Modeling of Surface Waves Based on Principal Equations of Potential Wave Dynamics. Technical Note.